

UNCLASSIFIED

AD 408 915

DEFENSE DOCUMENTATION CENTER

FOR

SCIENTIFIC AND TECHNICAL INFORMATION

CAMERON STATION, ALEXANDRIA, VIRGINIA



UNCLASSIFIED

NOTICE: When government or other drawings, specifications or other data are used for any purpose other than in connection with a definitely related government procurement operation, the U. S. Government thereby incurs no responsibility, nor any obligation whatsoever; and the fact that the Government may have formulated, furnished, or in any way supplied the said drawings, specifications, or other data is not to be regarded by implication or otherwise as in any manner licensing the holder or any other person or corporation, or conveying any rights or permission to manufacture, use or sell any patented invention that may in any way be related thereto.

411 650

NOT SUITABLE FOR RELEASE TO OTS

①

No. 408 915

DDC FILE COPY

RESEARCH LABORATORIES

CESIUM PLASMA STUDIES FOR THERMIONIC ENERGY CONVERSION

Final Report, Phase II
Contract No. Nonr 3501(00)
Order No. 209-62, Task 399-358
June 1963

J. Y. Wada and R. C. Knechtli

408 915

JUL 10 1963

NOT SUITABLE FOR RELEASE TO OTS

Reproduction in whole or in part is permitted for
any purpose of the United States Government.

⑤ 418 630

HUGHES RESEARCH LABORATORIES
Malibu, California

a division of hughes aircraft company

⑦ 1.11
⑧ 2.11.11

⑥ CESIUM PLASMA STUDIES FOR
THERMIONIC ENERGY CONVERSION

Final Report, Phase II

⑬ Contract No. Nonr 3501(00)

⑭ HKHH Order No. 209-62, Task 3991358
June 1963

⑩ J. Y. Wada and R. C. Knechtli.
~~Electron Dynamics Department~~

⑪ Jan 63

⑫ 114.

⑬+⑭ NA

⑮+⑯ NA

⑰ 11

⑱ NP

SP

TABLE OF CONTENTS

	LIST OF ILLUSTRATIONS	v
I.	INTRODUCTION AND SUMMARY.	1
II.	CONCLUSIONS	3
III.	THERMALIZATION OF FAST ELECTRONS IN A HIGHLY IONIZED PLASMA: PART 1. METHODS OF MEASUREMENT AND LIMITATIONS	5
	A. Introduction.	5
	B. Apparatus for Plasma Generation and Electron Injection.	5
	C. Theoretical Computation of the Plasma Temperature under Conditions of Complete Thermalization of Injected Electrons	8
	D. Methods of Electron Temperature Measure- ments	12
IV.	THERMALIZATION OF FAST ELECTRONS IN A HIGHLY IONIZED PLASMA: PART 2. MEASURE- MENT OF PLASMA TEMPERATURE AND ESTIMATE OF DEGREE OF THERMALIZATION OF FAST INJECTED ELECTRONS	19
	A. Introduction.	19
	B. Measurement of Electron Thermalization in a Coulomb Collision Dominated Plasma	19
	C. Measurement of Electron Thermalization in a Collisionless Plasma	19
	D. Conclusions.	28
V.	THERMALIZATION OF FAST ELECTRONS IN A HIGHLY IONIZED PLASMA: PART 3. MEASURE- MENT OF THE NOISE SPECTRUM AND THEORY OF THE THERMALIZATION PROCESSES IN A COLLISION- LESS PLASMA	31
	A. Introduction.	31
	B. Theory of Electron-Plasma Wave Interaction and Resulting Thermalization	32
	C. Noise Spectrum Measurements.	46
		iii

VI.	ELECTRICAL RESISTIVITY OF A HIGHLY IONIZED CESIUM PLASMA.	57
A.	Method of Measurement	57
B.	Current-Voltage Characteristics between Plasma Emitters	59
C.	Measured Plasma Resistivity in the Absence of Ohmic Heating	66
VII.	FORMATION OF CESIUM PLASMA AND MEASUREMENT OF THE PROBABILITY OF NEUTRALIZATION K_n OF Cs^+ ON A TANTALUM SURFACE IN A ONE-EMITTER SYSTEM.	69
A.	Statement of the Problem	69
B.	Method of Measurement.	69
C.	Formation of Cesium Plasma in a One-Emitter System with a Floating Collector	71
D.	Experimental Evaluation of the Probability of Neutralization K_n of Cesium on Hot Tantalum.	76
	REFERENCES	81
	ABSTRACT CARDS	83
	DISTRIBUTION LIST	87

LIST OF ILLUSTRATIONS

Fig. 1.	Electron injection into cesium plasma through cathode sheath.	6, 7
Fig. 2.	Effect of electron injection current on injection cathode sheath.	9
Fig. 3.	Normalized curve for calculating T_p/T_e as a function of injection conditions.	13
Fig. 4.	Electron energy spectra	15
Fig. 5.	Typical single probe I-V characteristics	17
Fig. 6.	Comparison of measured and calculated electron temperature in plasma	20
Fig. 7.	Langmuir probe characteristics of collisionless plasma with injection of high energy electrons.	22
Fig. 8.	Probe measurement of electron temperature versus injection voltage.	23
Fig. 9.	Probe measurement of electron temperature versus plasma density for fixed injection voltage	24
Fig. 10.	Cesium plasma tube and associated apparatus for the measurement of microwave noise spectrum	26
Fig. 11.	Microwave measurement of plasma (electron) temperature versus injection voltage.	27
Fig. 12.	Microwave measurement of plasma (electron) temperature versus injection current.	29
Fig. 13.	Cesium plasma system	33
Fig. 14.	Typical dispersion characteristics of an electrostatic plasma wave in finite plasma column	34
Fig. 15.	Dispersion diagram for lowest order symmetrical mode of a plasma column in the presence of injected electrons	39
Fig. 16.	Expanded dispersion diagram for the symmetrical mode of a plasma column	40

Fig. 17.	Typical dispersion diagram for the mode of one angular variation of a plasma column with injected electrons	41
Fig. 18.	The dependence of the maximum growth rate of instability as a function of (ω_b/ω_p)	42
Fig. 19.	The behavior of the dispersion diagram for an electrostatic plasma wave mode as a function of the dimensions of the surrounding conductor	44
Fig. 20.	Cesium plasma generator instrumented with electron emitter, coaxial probes, and movable Langmuir probe	47
Fig. 21.	The measured noise spectrum (in presence of injected electrons) as a function of frequency.	49
Fig. 22.	The noise spectrum at low frequency limit obtained with a coaxial probe outside the plasma	51
Fig. 23.	Typical peaks of the low frequency noise spectrum observed outside the plasma column.	52
Fig. 24.	A schematic diagram of the floating movable probes used for partial suppression of the noise in a plasma	55
Fig. 25.	Effect of partial suppression of the oscillation on Langmuir probe I-V characteristics	56
Fig. 26.	Probe instrumented cesium plasma tube with two plasma emitters	58
Fig. 27.	Typical axial potential distribution for biased plasma emitters	60
Fig. 28.	Typical I-V characteristics of the cesium plasma tube with two plasma emitters	64
Fig. 29.	Slope of I-V characteristics for $I \rightarrow 0$ in cesium plasma tube with two plasma emitters	65
Fig. 30.	Measurement of resistivity of highly ionized plasma versus plasma density	67
Fig. 31.	One-emitter cesium plasma generator for the measurement of K_n of Cs^+ on tantalum surface	70
Fig. 32.	Axial potential distribution of the plasma column in a single emitter system	73

Fig. 33.	Comparison of the theoretical and experimental normalized plasma density as a function of the normalized emitter temperature for $n_+ \cong 6 \times 10^{10}$ and 1.5×10^{10} ions/cm ³	77
Fig. 34.	Probability of neutralization of Cs ⁺ on hot tantalum surface as a function of the emitter temperature . . .	79

I. INTRODUCTION AND SUMMARY

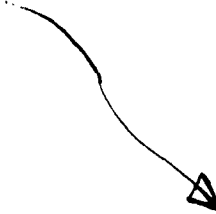
This report covers work on three separate subjects of interest to thermionic energy conversion and related to fundamental properties of plasmas:

1. Thermalization of fast electrons injected into a highly ionized plasma
2. Resistivity of a highly ionized plasma
3. Probability of neutralization of cesium ions on a hot tantalum surface.

The processes of thermalization of fast electrons injected into a plasma through a plasma sheath are investigated because such injection and thermalization are believed to occur in the plasma of the low voltage arc cesium plasma thermionic energy converter. Furthermore, it is believed that the injected electrons are thermalized at a faster rate than can be accounted for by random scattering through collisions with ions and neutrals. While this fast rate of thermalization is believed to be important to explain the low voltage cesium arc and more generally the ball of fire mode of discharge, the mechanism of thermalization is not yet understood. Therefore, the purpose of the present investigations on the thermalization of fast injected electrons is to measure the rate of energy transfer from fast injected to slow plasma electrons to establish conclusively whether thermalization takes place even in the absence of collisions and to determine the nature of the thermalization process.

The resistivity of highly ionized plasmas is investigated because it accounts for an important part of the internal voltage drop in thermionic energy converters, particularly when the internal resistive voltage drop is minimized by minimizing the effect of electron-neutral collisions. Unavoidable Coulomb collisions are then predominant, and the resultant plasma resistivity approaches that of a fully ionized plasma. The purpose of the investigations reported here is to measure the resistivity of a highly ionized plasma and to establish by these measurements the validity of the theoretical relations used to compute this resistivity. A further purpose is to obtain information on the Coulomb collision cross-section from these resistivity measurements in order to reliably determine the Coulomb collision mean free path in the thermalization experiments mentioned above.

* These conditions prevail in particular in the noble gas auxiliary discharge converters, where the effect of electron-neutral collisions is made negligible by the Ramsauer effect.



Investigations on the probability of neutralization of cesium ions on hot tantalum are reported here as a by-product obtained in using the cesium plasma apparatus developed for the other experiments conducted in the course of this ~~contract~~ work. These investigations are of interest for cesium plasma thermionic energy converters because the probability of neutralization of cesium ions on a hot refractory metal emitter affects the rate of ion loss, the economy of the discharge, and the potential distribution in such converters.³

II. CONCLUSIONS

The conclusions reached through the investigations outlined in Section I can be summarized as follows:

1. Energy transfer from fast electrons injected into a plasma to the slow electrons of this plasma takes place at a faster rate than can be accounted for by collisions. This results in thermalization of the injected electrons even when collisions are negligible.
2. The mechanism of energy transfer and thermalization in the absence of collisions seems to be a collective interaction between the fast injected electrons and a multiplicity of modes of electromechanical waves carried by the plasma electrons.
3. The resistivity of a fully ionized plasma is adequately predicted by Spitzer's equation, the measured values being within 35% of the theoretical values predicted by this equation.
4. The Coulomb collision cross-section for cumulative small angle deflections as calculated by Chandrasekhar and Spitzer is a good estimate of the actual cross-section, insofar as it has been found to lead to a valid theoretical expression for the plasma resistivity.
5. Experiments with a single emitter cesium plasma tube indicate consistently with earlier experiments (conducted with two emitter tubes) that the probability of neutralization of cesium ions on refractory metal surfaces and on tantalum in particular is substantially lower than predicted by the Saha-Langmuir equation.

III. THERMALIZATION OF FAST ELECTRONS IN A HIGHLY IONIZED PLASMA: PART 1. METHODS OF MEASUREMENT AND LIMITATIONS

A. Introduction

Our investigations on the thermalization of fast electrons injected into a highly ionized plasma are discussed in three sections. This first section (Part 1) describes the experimental apparatus, discusses the theoretical foundations upon which the interpretation of the measurements is based, and discusses the methods of measurement used in our investigations. The second section (Part 2) presents the experimental results of electron temperature measurements, which indicate effective thermalization of the injected electrons even when electron collisions are negligible. The third section (Part 3) presents a theory for the process of thermalization of fast electrons injected into a plasma. This theory results from the interpretation of the noise spectra measurements reported at the beginning of Part 3 and explains at least qualitatively the thermalization in collisionless plasmas observed in the measurements of Part 2.

B. Apparatus for Plasma Generation and Electron Injection

The apparatus for plasma generation and electron injection consists of a cesium plasma emitter facing an electron emitter (injection cathode) as illustrated in Fig. 1(a). In this apparatus a thermal cesium plasma is generated on a heated tantalum surface (1.27 cm diameter); the plasma is magnetically confined into a well-defined plasma column as shown schematically in Fig. 1(a). Electrons are injected into the plasma from the injection cathode, which is biased negatively with respect to the plasma emitter. The apparatus is operated so that the plasma assumes a potential nearly equal to the plasma emitter potential. Under such conditions (as shown in Figs. 1(b) and 1(c)), the potential difference between plasma emitter and injection cathode appears nearly all across the injection cathode sheath. Thus, the electrons emitted by the injection cathode are accelerated through this sheath and are injected into the plasma as an electron stream with a nearly monochromatic injection velocity corresponding to sheath voltage (injection voltage). A photograph of the apparatus sketched in Fig. 1(a) is shown in Fig. 1(d).

It is important that the injection cathode sheath be much smaller than the total length of the plasma column and remain that small even when electrons are injected into the plasma. The effect of the injected electrons on the injection cathode sheath thickness has therefore been estimated. Analysis has shown that the potential profile near the negatively biased cathode is not noticeably altered from the nonemitting condition as long as the injection current density is maintained below the random plasma electron current density. In this case there is no potential minimum in front of the injection cathode; it

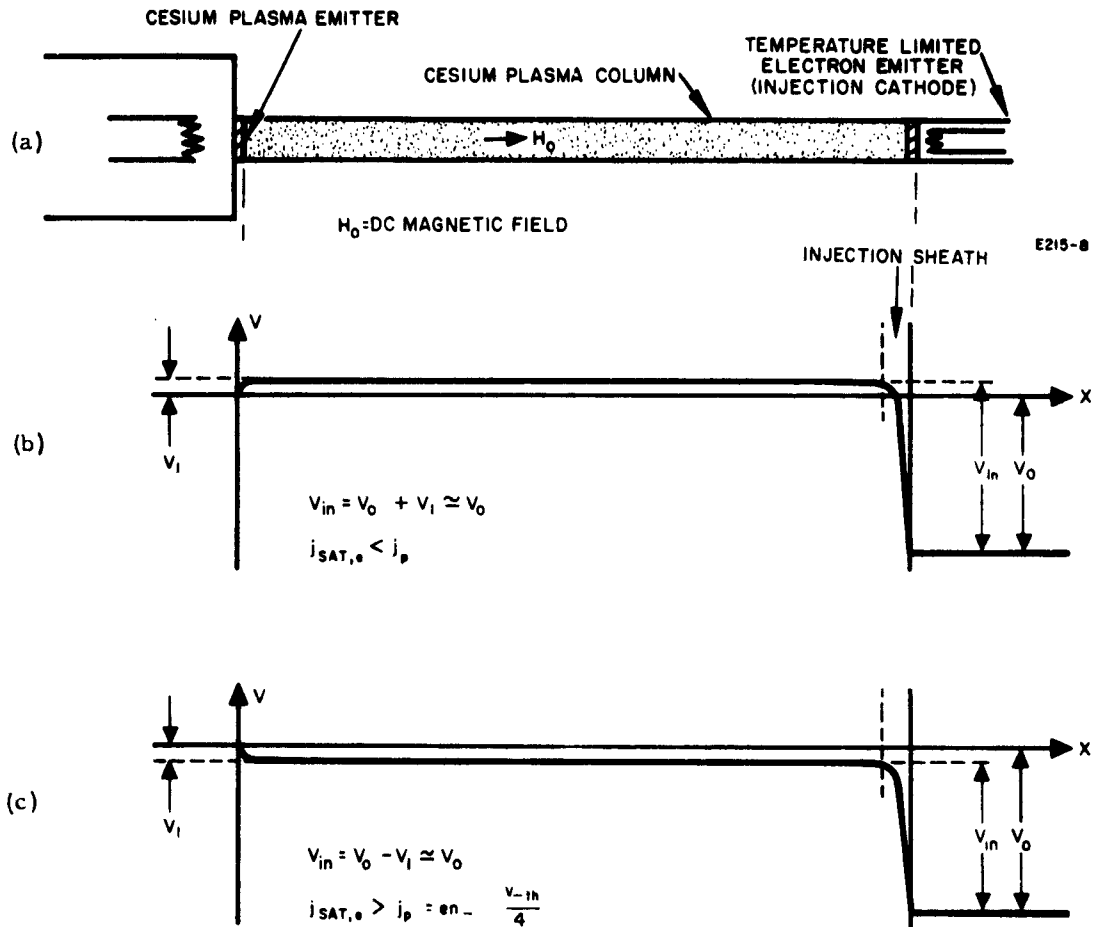


Fig. 1. Electron injection into cesium plasma through cathode sheath. (a) Apparatus. (b) Axial potential distribution for negative plasma emitter sheath. (c) Axial potential distribution for positive plasma emitter sheath.

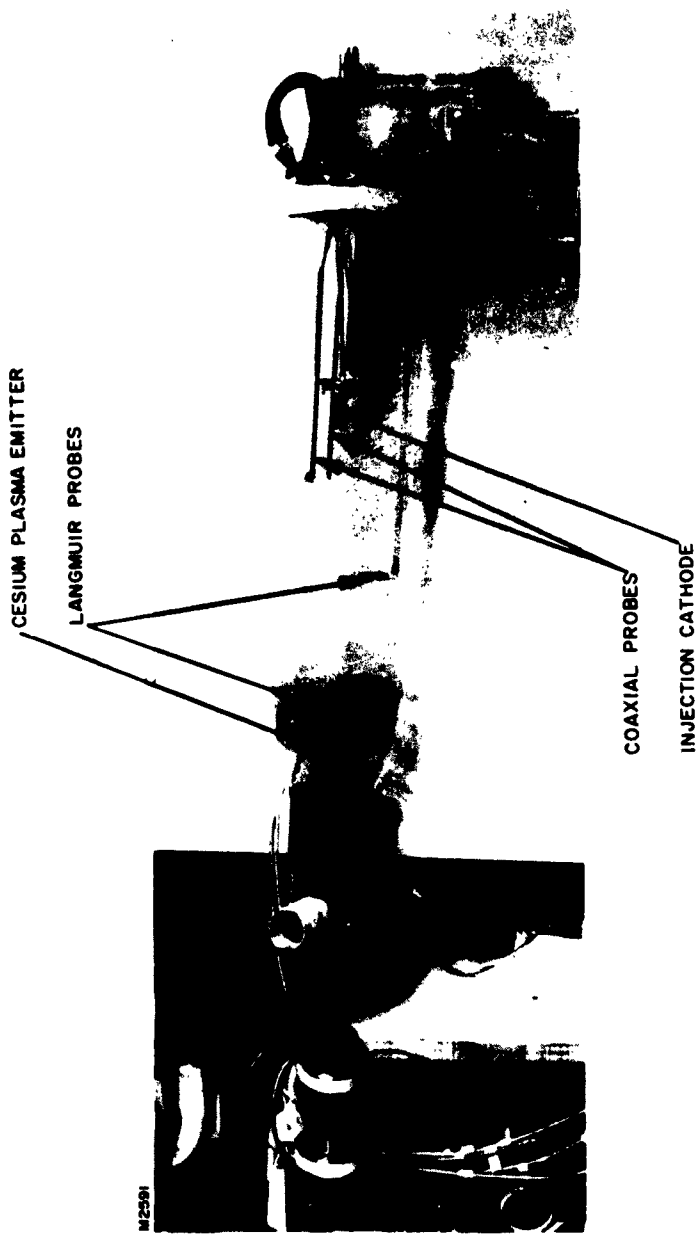


Fig. 1. (continued)
(d) Photograph of cesium plasma generator equipped with an injection cathode for the measurement of the thermalization of fast injected electrons into a plasma.

is temperature limited, and the injected current is controlled by the cathode temperature. The effect of injected electrons on the cathode sheath is illustrated for a typical case in Fig. 2. In this illustration, the cathode sheath potential (normalized with respect to the plasma electron temperature) is plotted against the distance (normalized with respect to the corresponding Debye length). It is clearly seen that the effect of the injection current is small and that the sheath thickness remains of the order of 20 times the Debye length, which for a typical thermal cesium plasma is smaller than 1mm. Compared with the length of the plasma column (approximately 30 cm), such a cathode sheath thickness is negligible. By using this method of plasma generation and electron injection, the magnitude of the injected current and the energy of the injected electrons can be regulated nearly independently from the plasma density and plasma electron temperature.

The electron energy distribution and the radiation from the plasma will be measured in this apparatus by methods discussed later (Section III-D). Furthermore, the electron energy distribution expected when the injected electrons are completely thermalized will be calculated in the next section. By comparing this calculated electron energy distribution with that measured, quantitative information on the degree of thermalization of the injected electrons will be obtained.

C. Theoretical Computation of the Plasma Temperature under Conditions of Complete Thermalization of Injected Electrons

In the following calculations, we assume that the fast injected electrons are completely thermalized and that the resultant electron energy distribution is Maxwellian. We shall now compute the temperature of this resultant electron energy distribution.

Consider the two axial plasma potential distributions shown in Figs. 1(b) and 1(c) for the cesium plasma column shown in Fig. 1(a). The cathode sheath thickness remains small since the injection electron current density from the cathode is maintained by temperature limited operation at such values that it is much smaller than the random current density available from the plasma. Under these conditions the plasma potential remains close to the plasma emitter potential. The potential difference between the plasma emitter and the injection cathode appears nearly all across the cathode sheath ($V_1 \ll V_{in}$). The potential distribution with a positive emitter sheath as shown in Fig. 1(b) is expected to exist when the saturation electron current through thermionic emission at the plasma emitter surface is smaller than the random plasma electron current available from the plasma column. This condition is usually found at high plasma densities. The potential distribution shown in Fig. 1(c) corresponds to the case where excess electrons are reflected back to the plasma emitter from the plasma column, the latter assuming a potential

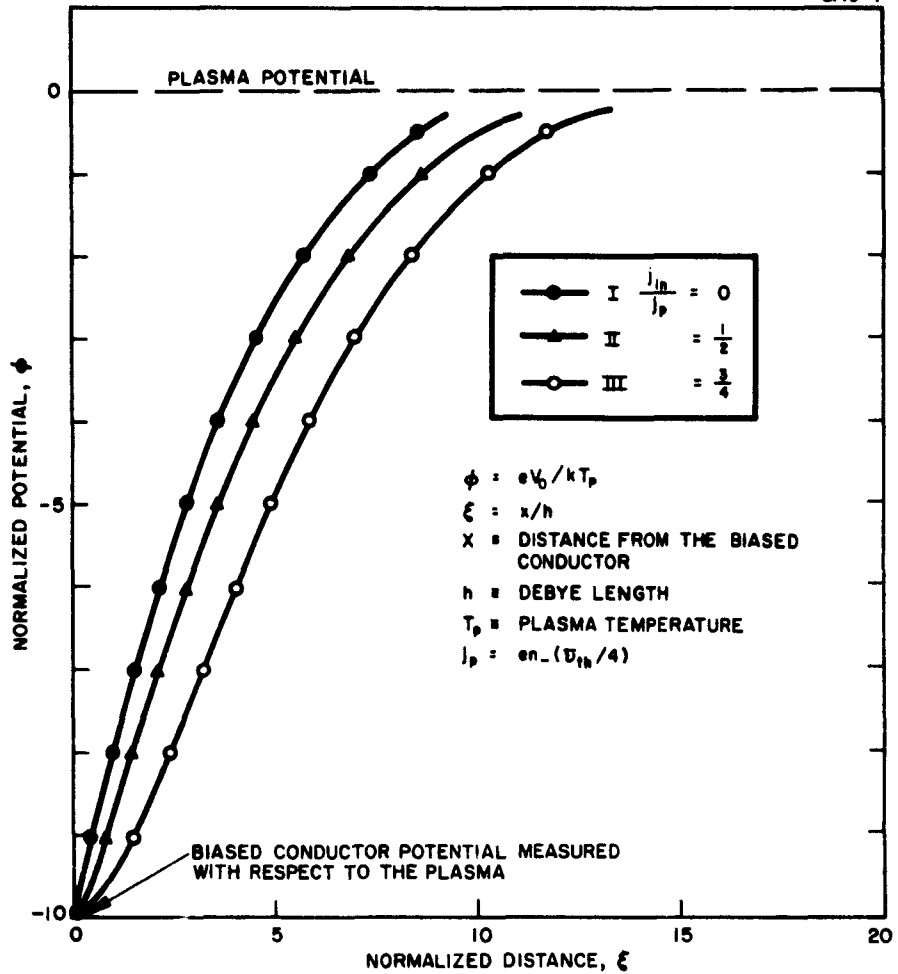


Fig. 2. Effect of electron injection current on injection cathode sheath. ($V_0 \approx V_{in}$).

slightly negative with respect to the plasma emitter surface. This latter condition is found in experiments performed at low plasma densities or high plasma emitter temperature, where the saturation electron current density available from the plasma emitter exceeds the random plasma electron current density. We shall now consider these two cases separately.

1. Plasma Electron Temperature for Positive Emitter Sheath (Fig. 1(b))

The basic equations to be used are those of conservation of electrons and of conservation of energy. These equations simply state that the rate of electron generation equals the rate of electron loss and that the power flow carried by electrons into the plasma equals the power flow carried by electrons out of the plasma. Energy transfer between electrons and ions or neutrals is neglected because of the small electron to ion mass ratio and of the limited number of collisions between electrons and ions or neutrals in our experiments.

a. Conservation of Electrons - For the conditions in which the rate of electron losses to the probes and by recombination is negligible compared with the loss of electrons escaping from the plasma back to the emitter, the equation of the conservation of electrons is simply

$$j_s + j_{in} = j_p \exp(-eV_1/kT_p) \quad (1)$$

where

j_s \equiv saturation current density available from the plasma emitter

j_{in} \equiv injected electron current density available from the negatively biased electron emitter

T_p \equiv plasma electron temperature

j_p \equiv $n_e \left(\frac{\bar{v}_{th}}{4} \right)$ \equiv random electron plasma current

\bar{v}_{th} \equiv mean thermal electron velocity

n_e \equiv electron density.

In writing (1) it is assumed that the plasma electron temperature and density are uniform over the entire plasma region.

b. Conservation of Energy - The equation for the conservation of energy with the potential distribution of Fig. 2(b) is

$$j_s \left(\frac{2kT_e}{e} \right) + j_{in} \left(V_{in} + \frac{2kT_{in}}{e} \right) = j_p \frac{2kT_p}{e} \exp(-eV_1/kT_p) \quad (2)$$

where T_{in} is defined as the temperature of the negatively biased electron emitter (injection cathode). V_{in} is the injection voltage, i.e., the potential difference between plasma and injection cathode surface. Since in our experiments $V_{in} \gg 2kT_{in}/e$,

$$\frac{2kT_e}{e} j_s + V_{in} j_{in} \cong \left(j_p \frac{2kT_p}{e} \right) \exp(-eV_1/kT_p) \quad (3)$$

The LHS of this equation represents the power flow carried into the plasma by electrons, whereas the RHS represents the power flow carried by electrons out of the plasma. Eliminating V_1 from (1) and (3) yields

$$\frac{T_p}{T_e} = \frac{\left[1 + \left(\frac{eV_{in}}{2kT_e} \right) \frac{j_{in}}{j_s} \right]}{\left(1 + \frac{j_{in}}{j_s} \right)} \quad (4)$$

It is noted that in the absence of the injected electrons ($j_{in} = 0$), the above relation reduces, as it should, to

$$T_p = T_e$$

These equations are consistent with the conservation equations used in previous investigations of cesium plasmas produced in a similar fashion.⁴

2. Plasma Electron Temperature for Negative Emitter Sheath

For the case in which the electron emission from the plasma emitter is greater than the random plasma current available from the plasma column the conservation equations become

Conservation of electrons:

$$j_s \exp(-eV_1/kT_e) + j_{in} = j_p \quad (5)$$

Conservation of energy:

$$\frac{2kT_e}{e} \left[j_s \exp(-eV_1/kT_e) \right] + V_{in} j_{in} = j_p \frac{2kT_p}{e} \quad (6)$$

Eliminating $j_s \exp(-eV_1/kT_e)$ from these equations and defining the random plasma current in the absence of the heating as $j_{po} = j_p$ ($T_p = T_e$), we obtain an expression from which the plasma temperature T_p can be calculated for the given injection conditions and plasma density:

$$\frac{j_{in}}{j_{po}} \left(\frac{eV_{in}}{2kT_e} \right) = \left[\frac{T_p}{T_e} \left(\frac{T_p}{T_e} - 1 \right) + \frac{T_p}{T_e} \left(\frac{j_{in}}{j_{po}} \right) \right] \quad (7)$$

The electron temperature T_p can be determined theoretically from a set of normalized curves obtained from (7) and shown in Fig. 3.

Equations (4) and (7) are the theoretical expressions with which experimental measurements of electron temperature as a function of injection parameters and plasma density will be compared later.

D. Methods of Electron Temperature Measurements

1. General Considerations

The investigations reported here are primarily limited to conditions where the injected electrons are fully or nearly fully thermalized. The resulting electron velocity distribution in the plasma therefore appeared sufficiently close to Maxwellian to permit characterizing the electron velocities by the temperature of the corresponding Maxwellian velocity distribution.

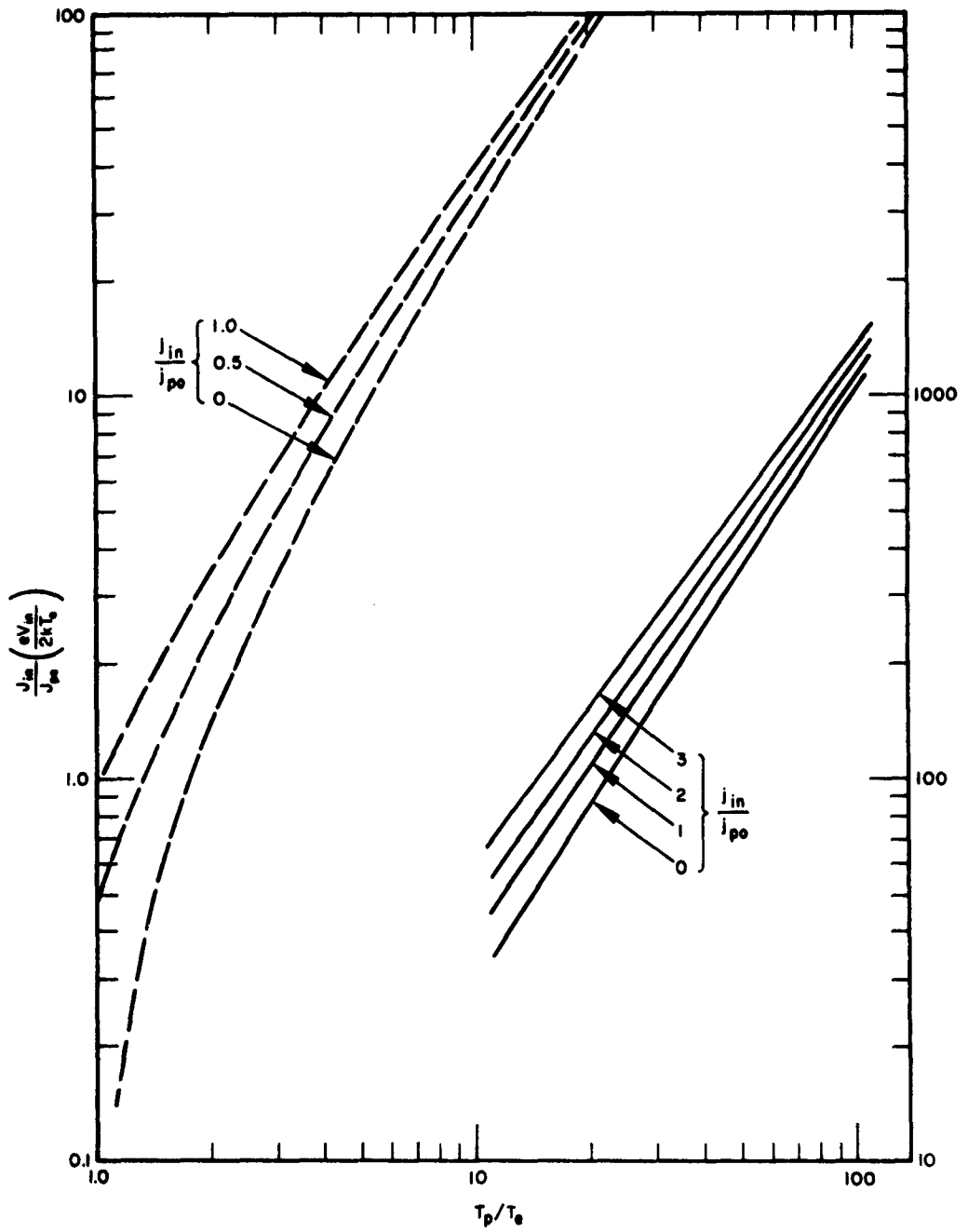


Fig. 3. Normalized curve for calculating T_p/T_e as a function of injection conditions (eq. (7)).

Two independent techniques were used to measure the electron temperature of the plasma as a function of electron injection parameters: (1) the Langmuir probe technique; (2) the microwave noise radiation technique.

It should be noted that these techniques yield unequivocal results only when the velocity distribution is isotropic (which is the case for a Maxwellian velocity distribution). In fact, the velocity distributions to be expected in our injection experiments are not necessarily Maxwellian; they will be determined by the rate and mechanism of energy transfer from the injected to the plasma electrons. The types of electron energy spectra expected for increasingly strong interaction between injected (fast) and plasma (slow) electrons are illustrated in Fig. 4. In the absence of injected electrons, the electrons are all generated at the plasma emitter, are in thermal equilibrium, and have a temperature equal to that of the plasma emitter. The electron energy spectrum contains only one peak and would be as shown by the solid curve in Fig. 4(a) without a second high energy peak. As energetic electrons are injected into this initially quiescent cesium plasma, the total electron energy distribution is modified and assumes a new steady state distribution determined by the rate of energy exchange between fast injected electrons and slow plasma electrons. In the absence of interaction between injected electrons and plasma electrons, the two classes of electrons would be unperturbed and the resulting spectrum would appear as sketched in a solid line in Fig. 4(a). When a relatively small energy transfer takes place between the injected and the plasma electrons, the spectrum would become distorted as shown by the dotted line in Fig. 4(a). The energy spread of the plasma electrons would increase (heating), the average energy of the injected electrons would decrease, and the energy spread of the injected electrons would probably increase. As the rate of energy transfer increases, plasma electrons and injected electrons are no longer clearly distinguishable, and a composite spectrum such as that shown in a solid line in Fig. 4(b) results. At the extreme limit, full thermalization takes place; the resulting velocity distribution again is Maxwellian, but with a temperature higher than the plasma emitter temperature. The energy spectrum is then as shown in the dotted line of Fig. 4(b). The experiments reported here correspond to conditions close to the strong interaction case.

2. Langmuir Probe Measurement

Langmuir probe measurements of the plasma electron temperature in the absence of the energetic injected electrons have been shown to be reliable, even in presence of the magnetic field used in our experiments.⁵ In such probe measurements, however, those electrons with relatively high energy are preferentially collected. They represent the high energy tail of the energy distribution function. When the total electron energy distribution of the system is Maxwellian, the measurement of this high energy tail results in a reliable measure of the plasma temperature.

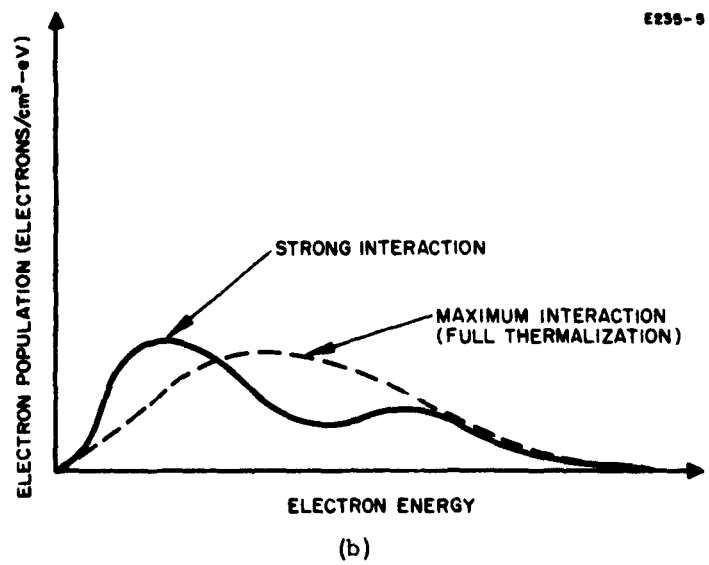
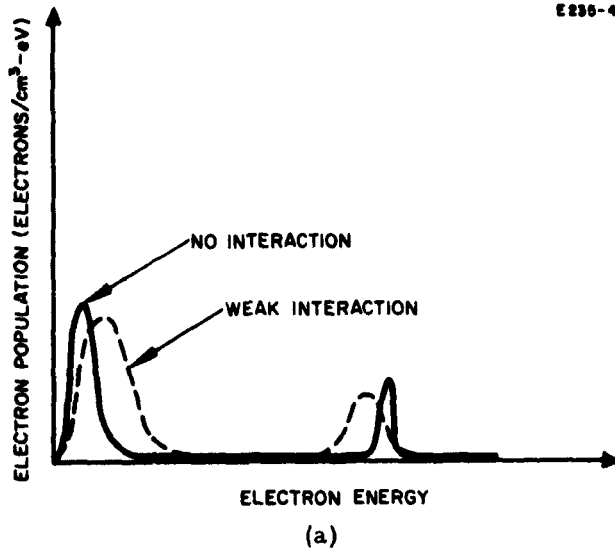


Fig. 4. Electron energy spectra.

When high energy electrons are injected into the plasma, probe characteristics such as those shown in Fig. 5 are obtained, and some caution is required to interpret them. To illustrate this, we consider the following example: If the distribution function is similar to the case of a strong interaction as shown by the solid line in Fig. 4(b), the measurement of the high energy electron distribution with a probe may look as shown by the solid line in Fig. 5(b) and result in an apparent Maxwellian distribution. However, these measurements will not be sufficient to indicate the nature of the spectrum at lower energies where, as shown again in Fig. 4(b), it may drastically differ from the Maxwellian distribution.

On the other hand, if the electron energy spectrum is similar to that shown in Fig. 4(a), the single probe measurement should yield an I-V characteristic as indicated by the solid line in Fig. 5(a). When the probe is biased strongly negative with respect to the plasma, most of the electrons, including the energetic injected electrons, are reflected, and only the ions are collected on the probe surface. As the probe potential is made less negative, the probe current will suddenly increase as the probe bias voltage nears the injection voltage of the injected electrons, the latter having most of their velocity in the axial direction. As the probe is made still less negative, the contribution from the plasma electrons eventually becomes important, and the effect of the injected electrons on these plasma electrons may be studied. Such measurements could, however, only show qualitatively that energy transfer does take place, because the electron velocity distribution in the presence of streaming electrons is nonisotropic in space and is not amenable to unequivocal probe measurement.

Should the rate of interaction between the fast electrons and the slow plasma electrons be stronger, leading to a Maxwellian energy distribution as shown in Fig. 4(b) (dotted lines), the probe characteristic would no longer indicate a step; it would show a smooth variation as shown by a solid line in Fig. 5(b). In an extreme case of complete thermalization, a quantitative measurement temperature determination is again possible. Experiments corresponding to the latter case have been performed and show reasonable agreement with theoretical expectations, as will be described in Section IV.

3. Microwave Thermal Radiation Measurements

The measurement of electron temperature by means of microwave radiation and its interpretation based on the classical radiation laws is known for a Maxwellian plasma. The absolute magnitude of the thermal radiation intensity in the microwave frequency range from electrons with a Maxwellian velocity distribution in a sufficiently dense plasma is equal to that of a black body with a temperature the same as that of the electrons.

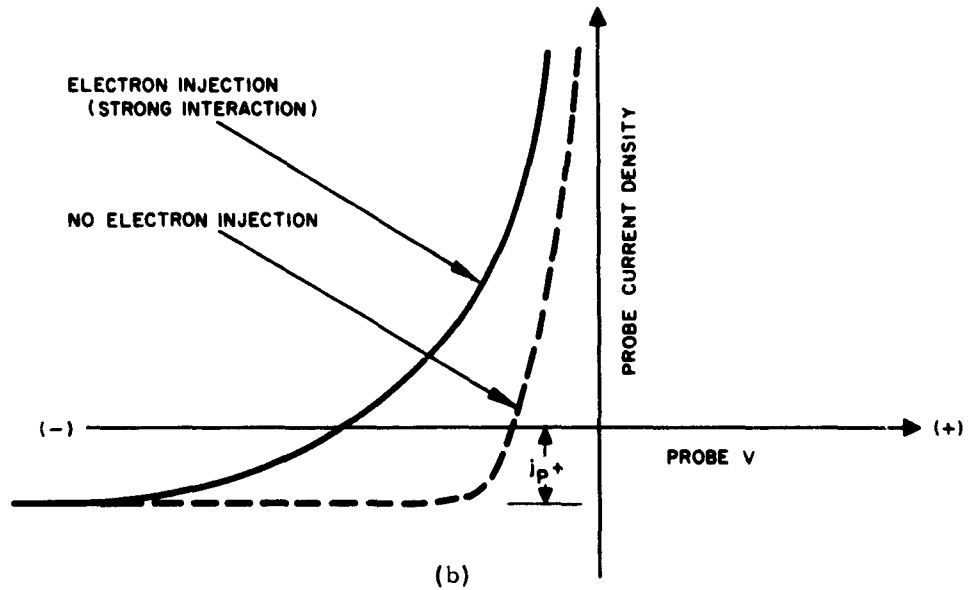
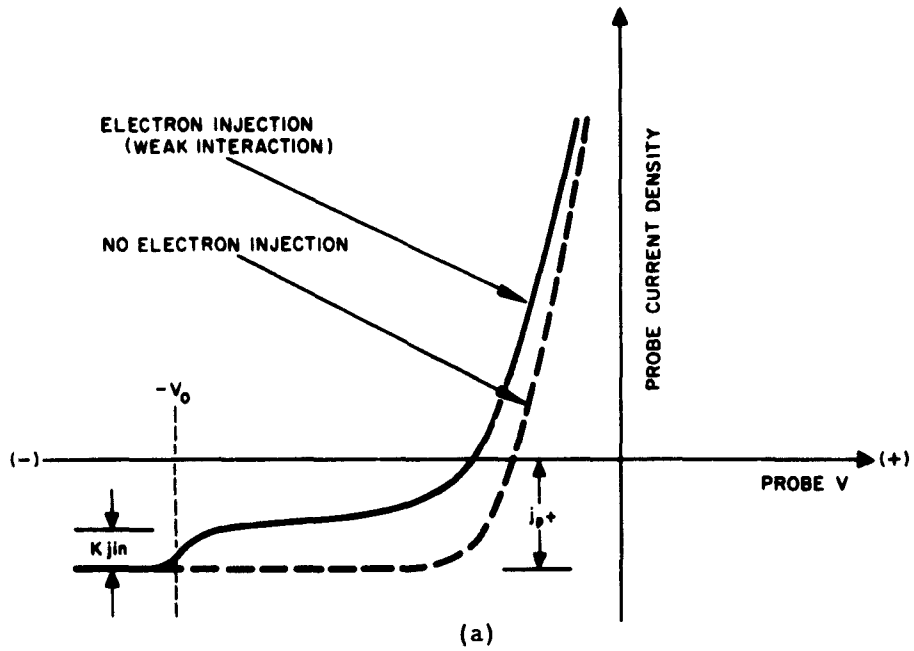


Fig. 5. Typical single probe I-V characteristics with and without injection of fast electrons ($V_0 \approx V_{in}$).

In the presence of injected electrons, however, great care must be taken in the interpretation of the microwave radiation measurement. As will be discussed in Part 3 (Section V), collective interactions between fast electrons and the plasma may occur. The radiation intensities at the frequencies where such collective interactions occur is expected to exceed the black body radiation by many orders of magnitude. The frequencies at which these enhanced radiations can occur are near or below the electron cyclotron and electron plasma resonance frequencies. The interpretation of these resonance radiation spectra is at best semiquantitative. Therefore, measurements at these resonance conditions should be avoided for quantitative temperature determination.

Further modification of the radiation intensity from a plasma may occur when the electron energy distribution differs from a Maxwellian distribution. For a weakly ionized non-Maxwellian plasma, the radiation near the cyclotron resonant conditions can differ considerably from that which would be observed in a Maxwellian plasma with electrons of the same average energy. The effective radiation temperature of the non-Maxwellian distribution at frequencies sufficiently remote from the cyclotron resonance, however, still approaches that of a black body of same temperature. The extension of such an observation in weakly ionized plasmas to a highly ionized plasma is not immediately apparent. However, if the radiation is modified because of a non-Maxwellian velocity distribution, as found in a weakly ionized plasma, it is reasonable to expect that radiation away from the cyclotron resonance may approach the black body radiation, as is the case in the weakly ionized plasma. It is therefore believed that microwave measurements of the average plasma electron temperature are relatively reliable, and do usefully supplement our probe measurements.

IV. THERMALIZATION OF FAST ELECTRONS IN A HIGHLY IONIZED PLASMA: PART 2. MEASUREMENT OF PLASMA TEMPERATURE AND ESTIMATE OF DEGREE OF THERMALIZATION OF FAST INJECTED ELECTRONS

A. Introduction

In the preceding section we have considered the method for measuring the degree of thermalization of fast electrons in a highly ionized cesium plasma; this method is based on comparison of the measured electron temperature with that calculated for the case of full thermalization. In this section we shall present the results of measurements of plasma electron temperature for various injection conditions and compare these results with the theoretical values predicted for the full thermalization of the injected electrons. Experiments have been performed for a Coulomb collision dominated plasma as well as for a collisionless case.

B. Measurement of Electron Thermalization in a Coulomb Collision Dominated Plasma

Langmuir probe measurements of electron temperature were performed on the apparatus sketched in Fig. 1 with probes located 3 cm from the plasma emitter, the total length of the plasma column being 30 cm. These measurements for the Coulomb collision dominated case have been described in detail in the Semi-Annual Technical Summary Report⁶ and will only be summarized here. The plasma electron temperature as a function of the injection current was obtained for a plasma density on the order of 2×10^{12} ions/cm³. The results of these measurements are shown in Fig. 6 together with the theoretical values calculated from (4). In this case, the Coulomb collision mean free path of injected electrons was comparable to or smaller than the length of the plasma. Thus, full thermalization of the injected electrons was expected. Under these conditions, the electrons in the plasma should assume a Maxwellian distribution; the probe measurement should be reliable; and the electron temperature predicted theoretically as a function of injection energy and current from (4) should be valid. Agreement between theory and experiment is seen in Fig. 6 to be reasonable.

C. Measurement of Electron Thermalization in a Collisionless Plasma

Measurements of the degree of thermalization of fast electrons in a collisionless plasma have been performed by means of both Langmuir probes and microwave techniques. We shall describe these measurements separately below.

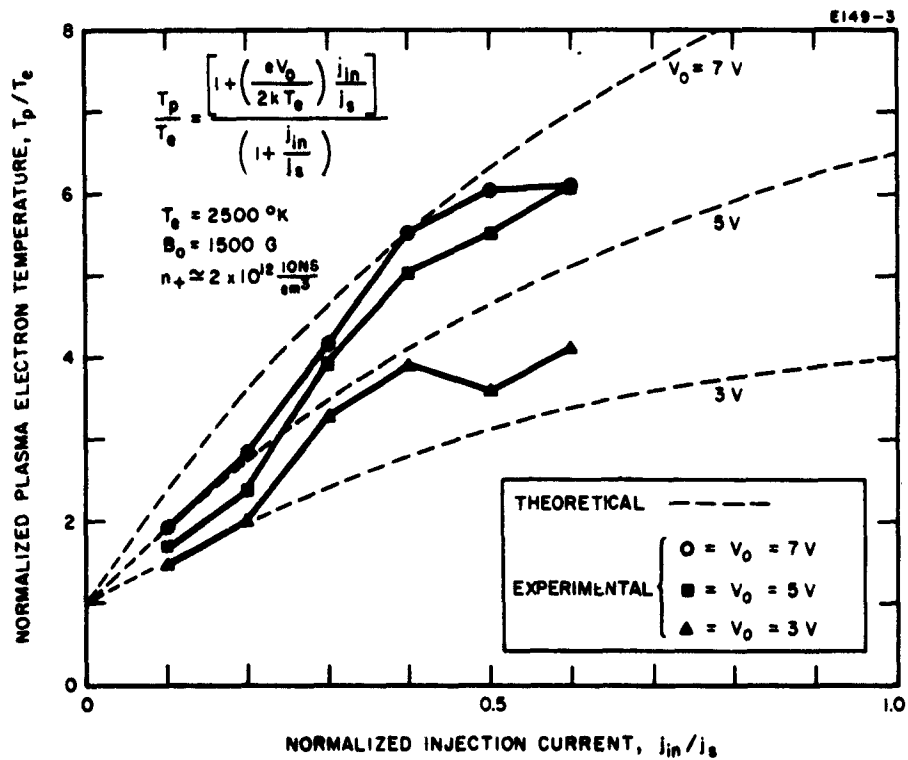


Fig. 6. Comparison of measured and calculated electron temperature in plasma with injection of fast electrons, for collision dominated case ($V_0 \approx V_{in}$).

1. Probe Measurements

The Langmuir probe measurements were performed with the same apparatus as the measurements reported in Section IV B, but at lower plasma densities. To study the collisionless case, these measurements were performed at a plasma density of the order of 10^9 electrons/cm³. At this density, the Coulomb collision mean free path for 1 eV electrons is of the order of 25 m, which is much larger than the 30 cm length of the plasma column. A set of single probe characteristics obtained for various injection energies is illustrated in Fig. 7. From such probe characteristics, the plasma electron temperatures have been determined and are shown in Figs. 8 and 9. The measurements of Fig. 8 show electron temperature as a function of injection voltage for a fixed plasma density of 1.3×10^9 electrons/cm³. The measurements of Fig. 9 show electron temperature versus plasma density for a fixed injection voltage of 40 volts. During all these measurements the plasma emitter temperature was maintained high enough to have $j_{\text{sat}} > j_p$ so that a negative sheath should form at the plasma emitter surface. The axial potential distribution corresponding to these conditions is given in Fig. 1(c), the theoretical value of the temperature for full thermalization is evaluated from (7) and is also shown in Fig. 8, together with the results of the previously mentioned probe measurements.

From Fig. 8 it is seen that the probe measurements of electron temperature agree reasonably well with the theoretical values up to an injection voltage of approximately 40 V. These measurements therefore indicate that practically complete thermalization of the fast electrons occurs in this energy range. As the injection energy is increased above 40 eV, it is observed that the conditions assumed in the theory are no longer applicable. In other words, the rate of energy exchange between the fast electrons and the slow plasma electrons is such that a complete thermalization of the fast injected electrons is no longer achieved. In this case, we could expect a double peak energy distribution function as shown in Fig. 4(a), and a step in the probe I-V characteristic (as indicated in Fig. 5(a)) should appear. The latter has, indeed, been observed from an injection voltage of about 40 eV up. One of the probe characteristics shown in Fig. 7 does show such a step, which is indicative of incomplete thermalization of the fast injected electrons. Such a step is observed and it increases as the injection energy is made higher. Qualitative interpretation of the probe measurements for the non-Maxwellian, nonisotropic velocity distribution apparent for $V_{\text{in}} > 40$ V is rather doubtful. Qualitatively, however, these observations are consistent with the expected behavior of the electron temperature as a function of the injection energy: when the fast injected electrons are not completely thermalized, the theoretical value given by (7) should predict larger electron temperatures than those observed. As the rate of energy transfer decreases, the discrepancy between the theoretical values of (7) and the measured temperatures should increase. Our observation is in agreement with this qualitative expectation. We have made attempts to estimate the fraction of the unthermalized portion of the injected electron current density from the magnitude of the step appearing in the I-V characteristic and have tried to account for the discrepancy

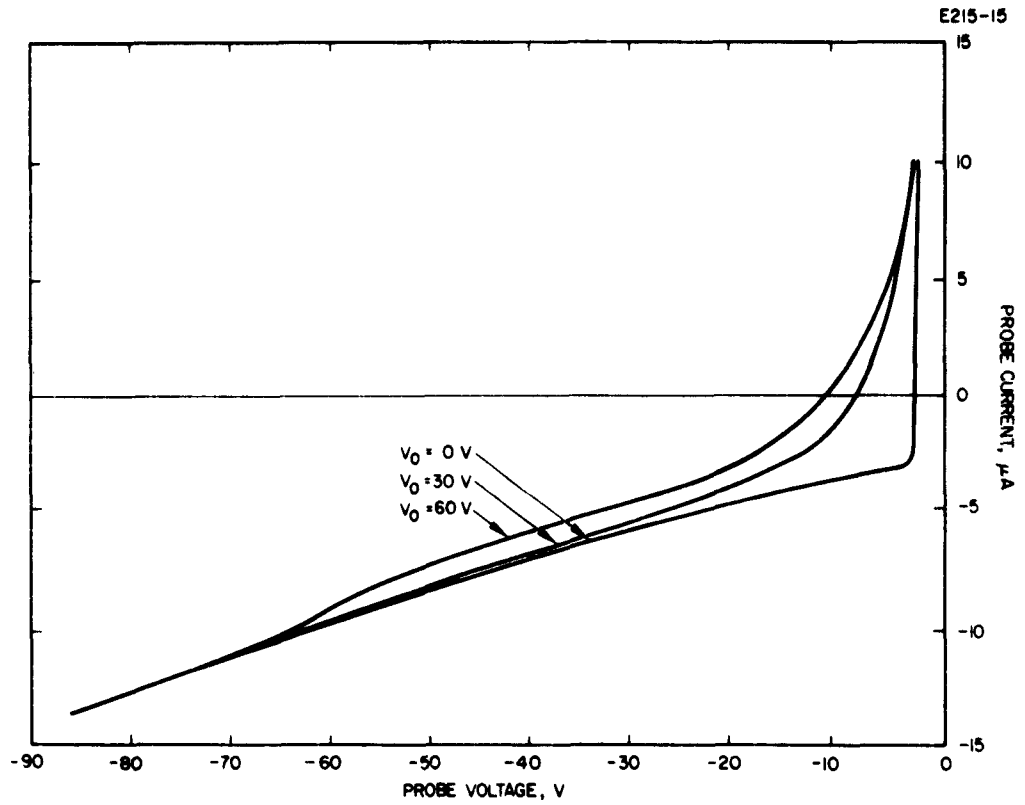


Fig. 7. Langmuir probe characteristics of collisionless plasma with injection of high energy electrons ($V_0 \approx V_{in}$).

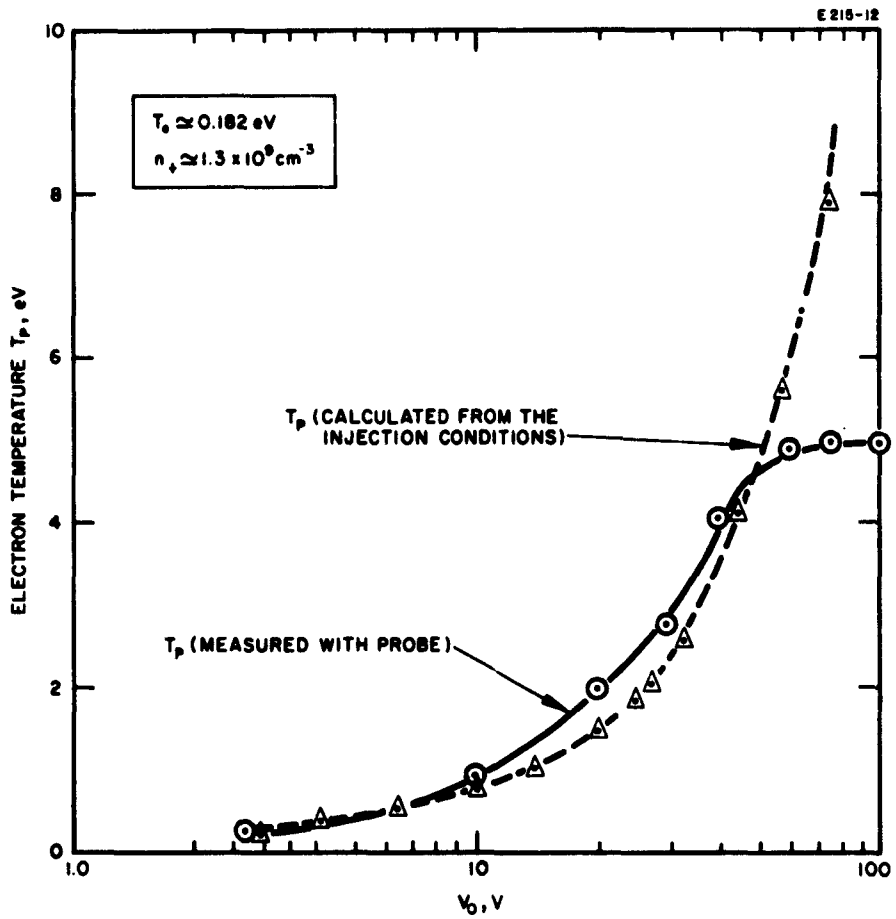


Fig. 8. Probe measurement of electron temperature versus injection voltage ($V_0 \approx V_{in}$).

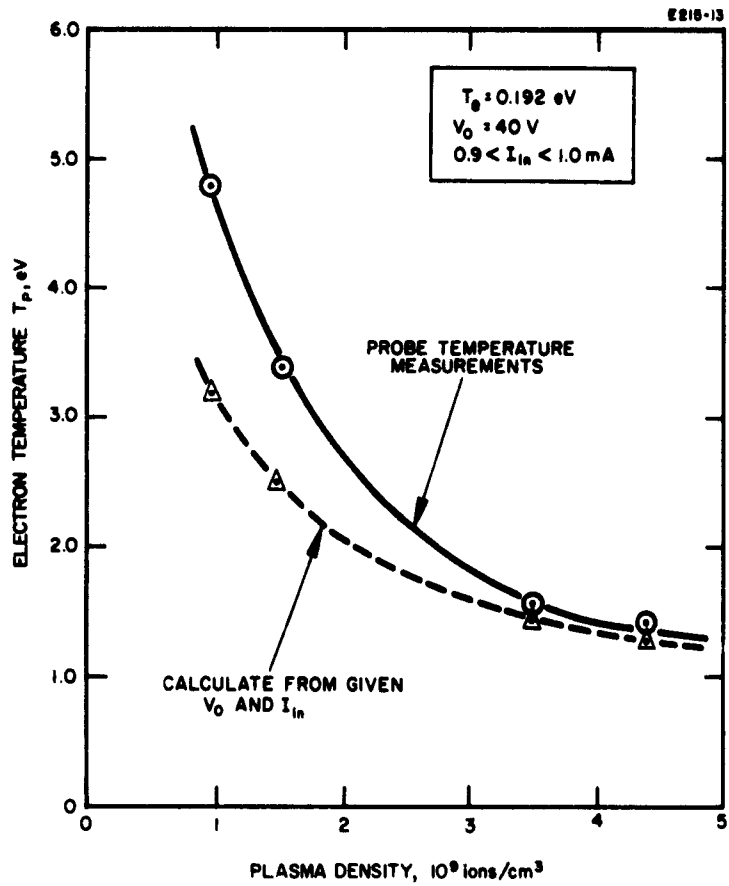


Fig. 9. Probe measurement of electron temperature versus plasma density for fixed injection voltage ($V_0 \approx V_{in}$).

observed between the measured and the calculated values. These attempts, however, were not very successful, the probe techniques being inadequate for the absolute measurement of the energy spectra of electrons under these conditions.* Even with these limitations, we can, however, conclude that the present results positively indicate (particularly for $V_{in} \leq 40$ V) a large degree of thermalization in a collisionless plasma. The energy exchange between fast injected electrons and slow plasma electrons under such conditions can be explained only through a collective interaction between the injected (fast) electrons and the plasma (slow) electrons. The nature of this interaction will be considered in Section V.

2. Microwave Noise Radiation Measurements**

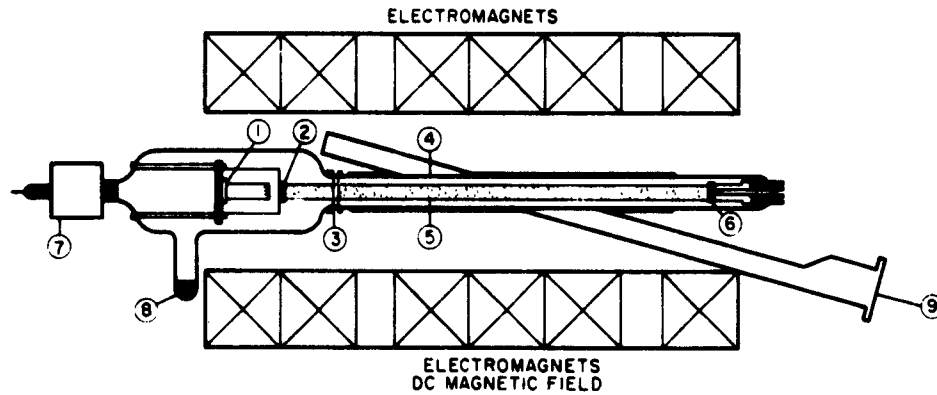
Microwave measurements of the plasma electron temperature have been made in a collisionless plasma using the apparatus sketched in Fig. 10. In these measurements, the noise spectrum has been measured as a function of the electron injection conditions for plasma densities of the order of 10^{10} electrons/cm³, an order of magnitude higher than those used in the preceding probe experiments. Even at this density, the Coulomb collision mean free path for electrons with 1 eV is still approximately 2.5 m. The plasma column in the present apparatus is 48 cm, which is much smaller than the Coulomb collision mean free path associated with energetic injected electrons. The principles of plasma generation and electron injections are the same as those described earlier in connection with Fig. 1.

For the measurement of the noise radiation intensities, the glass tubing containing the cesium plasma is placed diagonally in a reduced height S-band rectangular waveguide as shown in Fig. 10. When the plasma column is placed in the waveguide at a small angle, the radiated energy from the plasma can be measured directly, without need of correction due to poor coupling.

The radiation temperatures have been measured over a wide range of electron injection conditions. The effect of the injection energy on the plasma temperature has been investigated and results similar to those shown in Fig. 8 have been obtained and are shown in Fig. 11. Again, the comparison is made

* A new and improved method of measurement of electron energy distribution for energetic electrons injected into a plasma has been devised and is proposed to be used for the continuation of these investigations.

** The experimental results described in this section were performed by J. Y. Wada at the University of Southern California as a part of his Ph. D. dissertation. The cesium plasma tube used for these experiments at U. S. C. was built at Hughes Research Laboratories under this contract with the permission of Cdr. J. J. Connelly. Data are included in this report with the permission of Prof. Z. A. Kaprielian of the University of Southern California.



NO	NOMENCLATURE
1	CATHODE (FOR ELECTRON BOMBARDMENT HEATING).
2	TANTALUM DISC CESIUM PLASMA EMITTER (1.27 cm diameter)
3	LANGMUIR DOUBLE PROBE (0.025 cm diameter)
4	GLASS ENVELOPE (2.5 cm diameter)
5	PLASMA COLUMN (MAGNETICALLY CONFINED)
6	BIARIUM IMPREGNATED "L" CATHODE
7	VACUUM - ION PUMP
8	EXCESS CESIUM METAL
9	REDUCED HEIGHT S-BAND WAVEGUIDE WITH COUPLING HOLES FOR PLASMA COLUMN

Fig. 10. Cesium plasma tube and associated apparatus for the measurement of microwave noise spectrum.

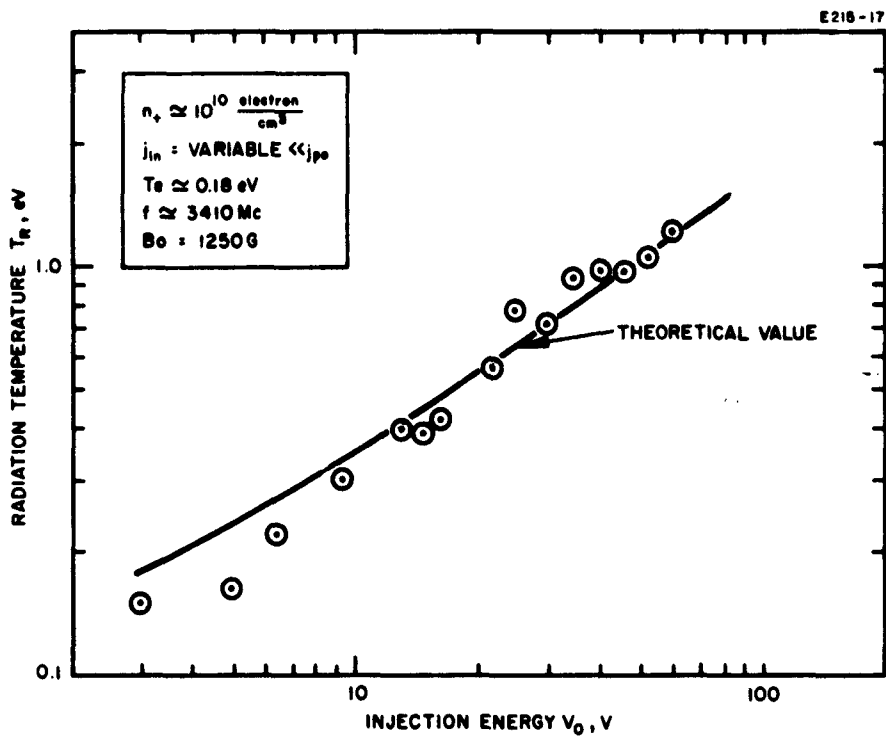


Fig. 11. Microwave measurement of plasma (electron) temperature versus injection voltage ($V_0 \approx V_{in}$).

with the theoretical values calculated from (7) for full thermalization. These noise measurements show excellent agreement with the theory derived for the complete thermalization of the fast electrons. Another comparison is made with the electron injection current as a variable, while the injection energy is maintained at 30 V; this is shown in Fig. 12. These measurements showed a consistent discrepancy of about 30%. Such an error may be introduced simply by overestimating the plasma density by 50%, which at these densities is quite possible. The agreement between the measured radiation temperatures and the calculated values again indicate that a strong energy exchange between fast electrons and plasma electrons exists and that the fast electrons are completely or nearly completely thermalized in the plasma.

As mentioned in the Section III, the radiation temperature equals the electron temperature of a plasma with a Maxwellian electron velocity distribution. However, the interpretation of the radiation intensities becomes difficult when the electron velocity distribution differs from a Maxwellian one. No quantitative analysis seems to exist for estimating the radiation from such a non-Maxwellian highly ionized plasma. For the present measurement, therefore, we have assumed that the radiation temperature is essentially equal to the plasma electron temperature. Another possible cause of errors in the interpretation of the present measurement may be the collective phenomena which may exist near the electron cyclotron and the electron plasma frequencies. The noise spectrum measurement near the electron cyclotron frequency, however, indicates that such phenomena are not important. Only a small peak (less than 50%) above the average noise intensity is observed near the cyclotron frequency. Since the plasma frequency was below the cutoff frequency of the waveguide, a large radiation (should it exist) near or below the plasma frequency would not affect the present noise radiation measurements.

These microwave radiation measurements thus lead to the same conclusion as the probe measurements, viz., that a high degree of thermalization of electrons is observed in the collisionless case and that energy exchange must be accomplished through collective interactions. The microwave measurement further indicates that collective interactions near the electron cyclotron frequencies are inoperative. The collective interactions thus must occur at frequencies other than the electron cyclotron frequency. This is consistent with qualitative radiation measurements at lower frequencies reported in Section V, indicating excess radiation below and up to the vicinity of the electron plasma frequency.

D. Conclusions

From the experimental results presented in this section, we conclude the following:

1. Both probe measurements and microwave noise radiation measurements positively indicate a high degree of thermalization of fast electrons injected into a collisionless plasma.

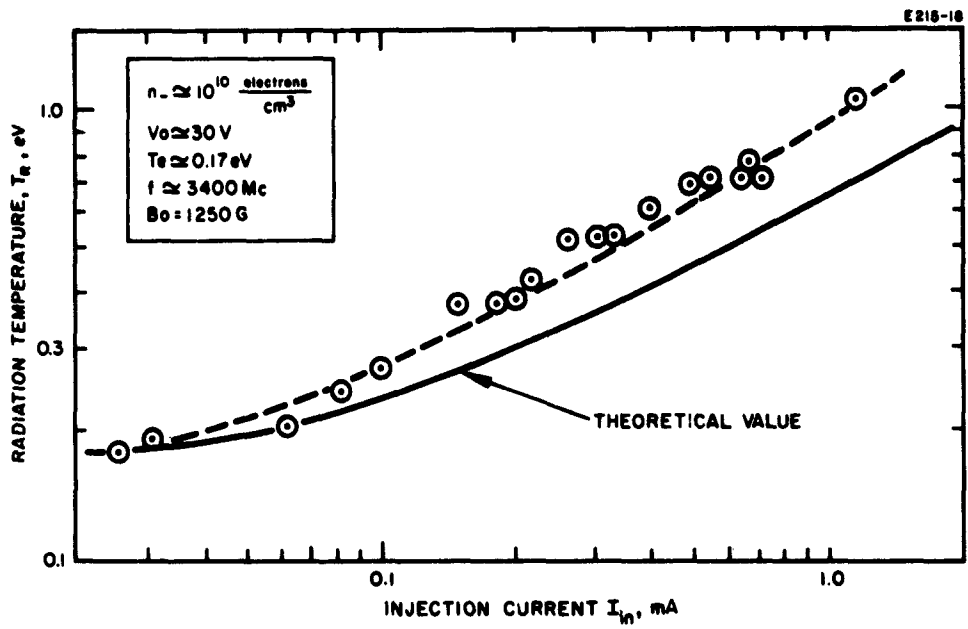


Fig. 12. Microwave measurement of plasma (electron temperature versus injection current ($V_0 \approx V_{in}$)).

2. In order to explain the observed rate of energy exchange between the fast injected electrons and the slow plasma electrons, collective electron interactions must be present;
3. Such collective interactions are not observed at or near the electron cyclotron frequency for an injection energy up to 100 eV.

It will be shown in the following section that further spectral measurement of the noise radiation suggests a collective electron-electrostatic plasma wave interaction. Also, it will be shown that this collective interaction could qualitatively explain the fast thermalization observed in the probe and microwave measurements reported above.

V. THERMALIZATION OF FAST ELECTRONS IN A HIGHLY IONIZED PLASMA; PART 3. MEASUREMENT OF THE NOISE SPECTRUM AND THEORY OF THE THERMALIZATION PROCESSES IN A COLLISIONLESS PLASMA

A. Introduction

The experimental results reported in Section IV and above show conclusively that a high degree of thermalization of fast electrons injected into a plasma takes place even in the absence of collisions: the injected energetic electrons are thermalized at a rate much faster than can be accounted for by random scattering through collisions with neutrals and plasma electrons and ions.

The following phenomena, which may cause the thermalization of energetic electrons injected into a collisionless plasma, are considered for the present experiments:

1. Electron-plasma wave interactions^{7, 8}
2. Electron-ion wave interactions⁹
3. Cyclotron-wave interactions¹⁰

These interactions can conceivably lead to instabilities and to the amplification of perturbations in the electron stream; they may lead to the thermalization of the energy of the injected electrons.⁸

To determine which, if any, of these interactions predominate, we have performed a series of spectral measurements of the noise radiation and oscillation spectrum. Excess noise is generated in the plasma over a wide frequency range when energetic electrons are injected into the initially quiescent and thermal cesium plasma. We were furthermore able to establish a correlation between controllable changes in the noise spectrum and changes in the electron energy distribution measured by Langmuir probes. On the basis of these observations we have concluded that electron-plasma wave interactions between the fast injected electrons and the slow plasma electrons were the predominant cause for thermalization of the injected electrons.

For the sake of clarity, we shall first discuss the theory of electron-plasma wave interactions. Experimental data on noise spectra will then be reported and shown to be consistent with this theory.

B. Theory of Electron-Plasma Wave Interaction and Resulting Thermalization

1. Physical Model and Method of Analysis

The electron-plasma wave interaction can be considered as a two-stream instability and is simple to explain qualitatively.^{7, 11} Assume that a small fluctuation is present in the plasma. This fluctuation will excite a plasma wave which propagates according to the dispersion relation characteristic of geometry and plasma distribution considered. This wave will be amplified if an appropriate number of the injected electrons have velocities nearly that of the phase velocity of this plasma wave. The conditions required for the growth of these instabilities or plasma waves can be calculated on the basis of a linearized theory. This first order theory predicts an exponential growth of the fluctuations. As the amplitude of these fluctuations increases, large signal conditions prevail and the linearized theory no longer applies. Under these large signal conditions, the injected fast electron stream carries a large amplitude modulation. However, this large amplitude modulation is unstable and breaks up rapidly, resulting in a randomization of the velocities of the injected electrons.^{8, 12} In other words, small fluctuations of the injected electrons are amplified by interaction with a plasma wave near synchronism, grow to large amplitudes, become unstable, break up, and result in the randomization of the originally monochromatic energy of the injected electron stream within a few plasma periods.⁸

2. Plasma Waves in Cylindrical Plasma Column

We shall first describe the possible mode of plasma wave propagation in a cylindrical plasma column surrounded by a conductor, such as is found in our experiments. The conductor, which is shown in Fig. 13, represents the rf shielding conductor placed around the apparatus. For the magnetic field applied in our experiments, the plasma column is confined to a well-defined radius "a." A number of electrostatic plasma wave modes can exist in this plasma system.¹³ A typical phase characteristic for an axially symmetrical mode where the electron cyclotron frequency ω_c is greater than the electron plasma frequency ω_p is illustrated by solid lines in the ω - β diagram of Fig. 14. As shown, the wave propagates for all frequencies below ω_p ; a pass band is also found near ω_c . We shall limit our consideration to the former. Any fluctuation produced in the plasma with a frequency in one of the pass bands propagates with a phase velocity $v_\phi = \omega/\beta$ along the plasma column. The maximum velocity $v_\phi \text{ max}$ for $\omega \leq \omega_p$ at which the wave can propagate in this typical mode is found according to this ω - β diagram for $\omega \rightarrow 0$.

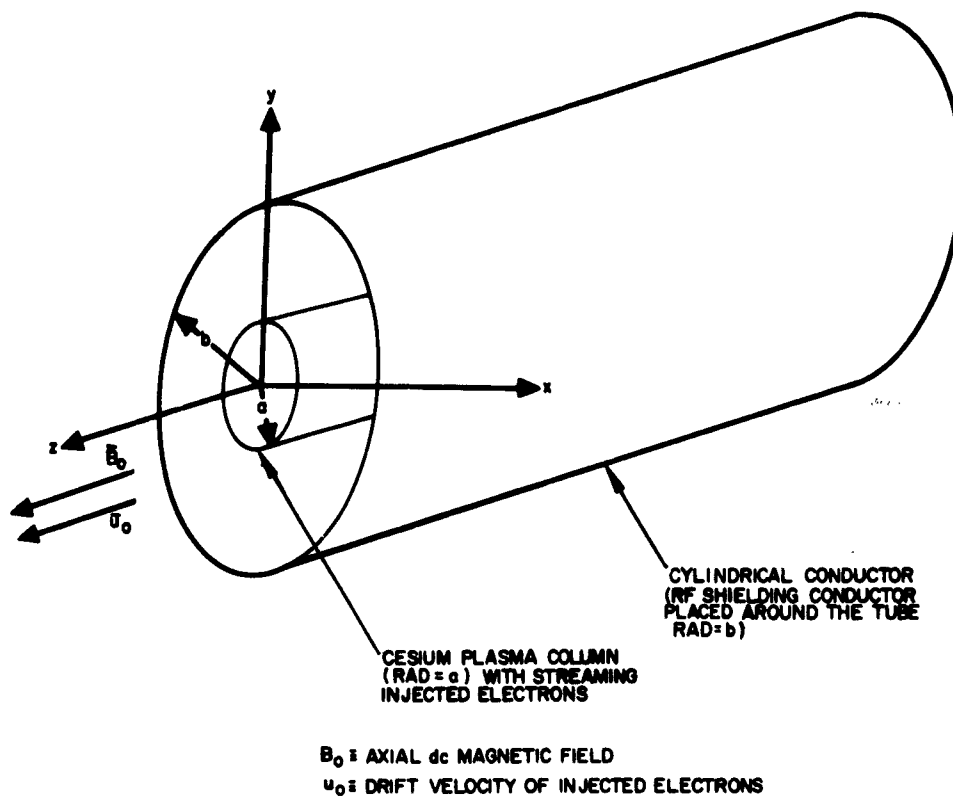


Fig. 13. Cesium plasma system.

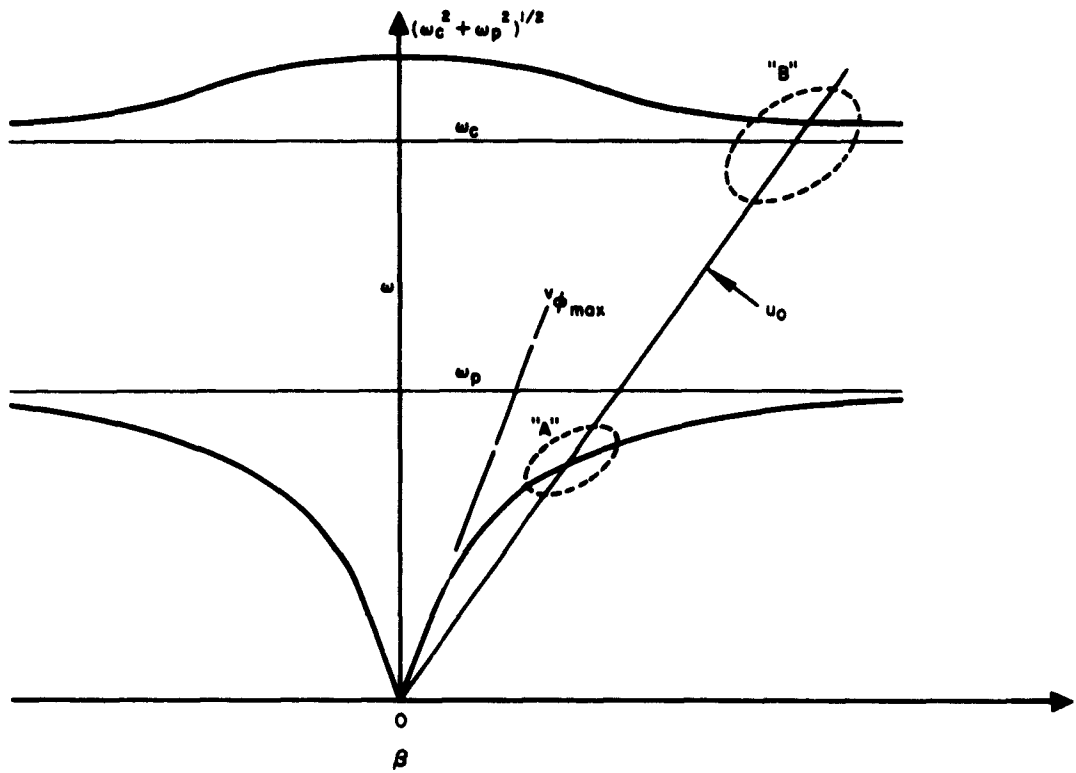


Fig. 14. Typical dispersion characteristics of an electrostatic plasma wave in finite plasma column.

The exact ω - β diagram for the various modes can be obtained from the following dispersion equation¹³:

$$\epsilon_{rr} T a \frac{J'_n(Ta)}{J_n(Ta)} - j n \epsilon_{r\theta} = \beta a \left[\frac{I'_n(\beta a) K_n(\beta b) - I_n(\beta b) K'_n(\beta a)}{I_n(\beta a) K_n(\beta b) - I_n(\beta b) K'_n(\beta a)} \right] \quad (8)$$

where

$a \equiv$ plasma radius

$b \equiv$ conductor radius

$$\begin{aligned} \epsilon_{rr} &\equiv \left(1 - \frac{\omega_p^2}{\omega^2 - \omega_c^2} \right) \\ \epsilon_{r\theta} &\equiv \frac{-j \omega_c \omega_p^2}{\omega(\omega_c^2 - \omega^2)} \\ T^2 &\equiv -\beta^2 \frac{(\omega^2 - \omega_p^2)(\omega^2 - \omega_c^2)}{\omega^2(\omega_p^2 - \omega_c^2)} \end{aligned} \quad (9)$$

and $J_n(\beta a)$, $K_n(\beta a)$, and $I_n(\beta a)$ are Bessel functions.

The above dispersion equation corresponds to the longitudinal electrostatic plasma waves. The following equations describe the electric field inside and outside: For the inside of the plasma ($r < a$)

$$E_z = C_1 J_n(Tr) e^{j(\omega t - \beta z + n\theta)} \quad (10)$$

and for the outside of the plasma ($a < r < b$)

$$E_z = C_2 \left[I_n(\beta r) K_n(\beta b) - I_n(\beta b) K_n(\beta r) \right] e^{j(\omega t - \beta z + n\theta)} \quad (11)$$

where θ represents the angular dimension and C_1 and C_2 are arbitrary constants.

Solution of the above dispersion equation for higher order modes would require extensive computer calculations. For the purpose of explaining our experimental results, however, a simpler first order solution (which does not affect the basic process involved) will be sufficient. Therefore, we shall in the following consideration solve the dispersion equation for the condition where the plasma fills the conducting cylinder.

We shall further limit our considerations to the condition which prevailed in our experiments, i. e., $\omega^2 \gg \omega_p^2$. This condition is satisfied since the magnetic field was such that $\omega_c/2\pi \geq 3000$ Mc, whereas the plasma density was such that $\omega_p/2\pi = 300$ Mc. The above dispersion equation then simplifies to the following form:

$$\frac{p_{nv}^2}{-(\beta a)^2} = \left(1 - \frac{\omega_p^2}{\omega^2}\right) \quad (12)$$

where p_{nv} is the ν^{th} root of $J_\nu(x) = 0$. This simplified dispersion equation will be used in the next section to analyze the interaction between electrons injected into the plasma and the electrostatic plasma waves.

3. Electron-Plasma Wave Interaction — Growing Wave Instability

Consider a group of streaming electrons with a velocity u_0 corresponding to that of the injection energy V_{in} . Shown in Fig. 14 is a line representing the electron beam velocity u_0 . Near the intersection of these ω - β and u_0 curves, the plasma wave's phase velocity is close to that of the drifting electrons; a strong interaction between the wave and the drifting electrons should occur and result in a condition favorable to two-stream instability.

It can be seen from Fig. 14 that an intersection of the ω - β curve and the electron beam velocity line exists for all values of u_0 smaller than the maximum phase velocity $v_{\phi \max}$ associated with the plasma wave mode considered. From (12) we obtain

$$v_{\phi \max}|_{nv} = \frac{\omega_p a}{p_{nv}} \quad (13)$$

The numerical values of $v_{\phi \max}|_{nv}$ are tabulated in Table I for the values found in our experiments ($f_p = 300$ Mc and $a = 0.65$ cm). If, for example, the electrons are injected into a plasma surrounded by a conductor with an initial velocity of $u_0 = 10$ eV, there will be five

modes (p_{00} , p_{10} , p_{20} , p_{30} , and p_{01}) for which intersections of the ω - β and u_o curves exist. These modes all can contribute to the thermalization of the injected electrons.

TABLE I

Maximum Phase Velocity v_{\max} of Higher Order Mode Electrostatic Plasma Waves; v_{\max} is Expressed in Electron Volts, in Terms of the Kinetic Energy of an Electron Having the Velocity v_{\max}
 $J_n(x) = 0$

ν	$J_0(p_{0\nu}), eV$	$J_1(p_{1\nu}), eV$	$J_2(p_{2\nu}), eV$	$J_3(p_{3\nu}), eV$	$J_4(p_{4\nu}), eV$
1	$v_{\phi\max} = 83$	29	16.3	10.6	5.6
2	14.2	8.7	6.1	4.6	3.4
3	5.7	4.2	3.2	2.5	2.1
4	3.1	2.4	2.0	1.62	1.4
5	1.95	1.6	1.4	1.2	1.1

Plasma characteristics: $f_p = 300$ Mc
 $a = 0.65$ cm

To consider this interaction more quantitatively, we shall include the effect of the injected beam in the dispersion equation. The previous equation then takes the following form:

$$\frac{p_{nv}^2}{-(\beta a)^2} = 1 - \frac{\omega_p^2}{\omega^2} - \frac{\omega_b^2}{(\beta u_o - \omega)^2} \quad (14)$$

where

$u_o \equiv$ the velocity of the injected electrons streaming in the plasma

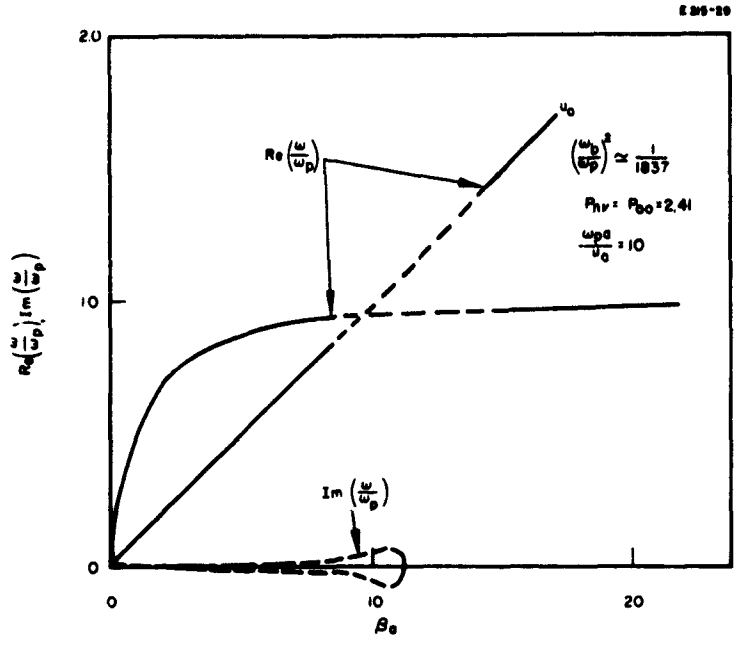
$\omega_b \equiv$ the plasma frequency associated with the streaming electrons.

The solutions to this dispersion equation have been evaluated for a number of limited conditions. To make use of the numerical solution available in a published paper,¹⁴ the computation was made for $(\omega_b/\omega_p)^2 = 1/1837$. Typical results obtained for the two assumed values of $\omega_p a/u_0$ (10, 5) for the axially symmetrical mode ($p_{nv} = p_{00}$) are shown in Figs. 15 and 16. These results were obtained by assuming that βa is real and by computing the real and the imaginary part of the frequency. As shown in Fig. 15(a) and 15(b), $\text{Im}(\omega/\omega_p)$ has a maximum value for the $\text{Re}(\omega/\omega_p)$ nearly equal to unity. This implies that, for these conditions, fluctuations having real frequencies near ω_p would have the fastest growth rate.

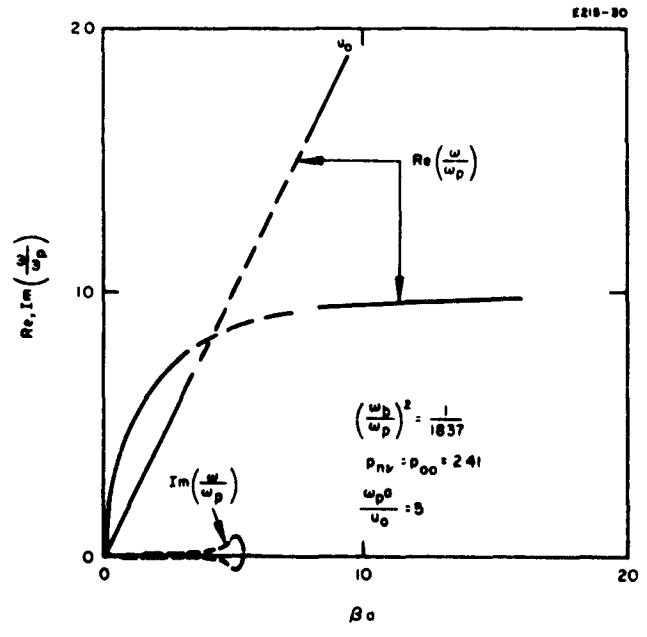
It is quite significant to observe that the $\text{Im}(\omega/\omega_p)$ is present for all values of $\text{Re}(\omega/\omega_p) \leq 1$, although the rate of growth ($\text{Im}(\omega/\omega_p)$) decreases monotonically with ω as shown in Fig. 16. This implies that even low frequency fluctuations ($\text{Re}(\omega/\omega_p) \ll 1$) would grow in due time, perhaps to a nonlinear limit, and might contribute to the large signal modulation aid to the thermalization of the injected electrons. This also implies that these fluctuations at low frequencies should contribute greatly to the enhanced noise level observable in a system. We shall examine these statements in more detail later when the measured noise spectra will be considered.

A similar calculation of $\text{Im}(\omega/\omega_p)$ has been made for the mode which exhibits an angular variation p_{10} . As shown in Fig. 17, the growth ($\text{Im}(\omega/\omega_p) > 0$) can occur for all $\text{Re}(\omega/\omega_p) \leq 1$. The results obtained in this calculation are essentially similar to those already described for the symmetrical mode. It is important to note, therefore, that every mode which exhibits the growing instability can contribute to the eventual randomization of the injected electrons if the amplitude of the growing fluctuation reaches the nonlinear limit.

The above calculations were made for a rather small value of the ratio of the injected beam plasma frequency to the slow electron plasma frequency ($\omega_b^2/\omega_p^2 = 1/1837$). The estimate of the effect of changing such a ratio on the maximum growth rate has been made. Here again, we make use of the results published by Bernstein and Trehan.¹⁴ By using a simple transformation of our dispersion equation (eq. (14)) and by making a comparison with the above paper,¹⁴ we have obtained Fig. 18 from which the maximum growth rate as a function of ω_b^2/ω_p^2 can be evaluated. The parameter $\beta_m a$ which appears in Fig. 18 is the value of βa at which the maximum $\text{Im}(\omega/\omega_p)$ occurs. For most purposes, this value ($\beta_m a$) corresponds to the intersection of the ω - β diagram of the p_{n1} mode of the plasma column and the u_0 line representing the injected electrons. As shown, no large increase of the max $\text{Re}(\omega/\omega_p)$ is achieved by increasing $(\omega_b/\omega)^2$ by an order of magnitude.



a.



b.

Fig. 15. Dispersion diagram for lowest order symmetrical mode of a plasma column in the presence of injected electrons.

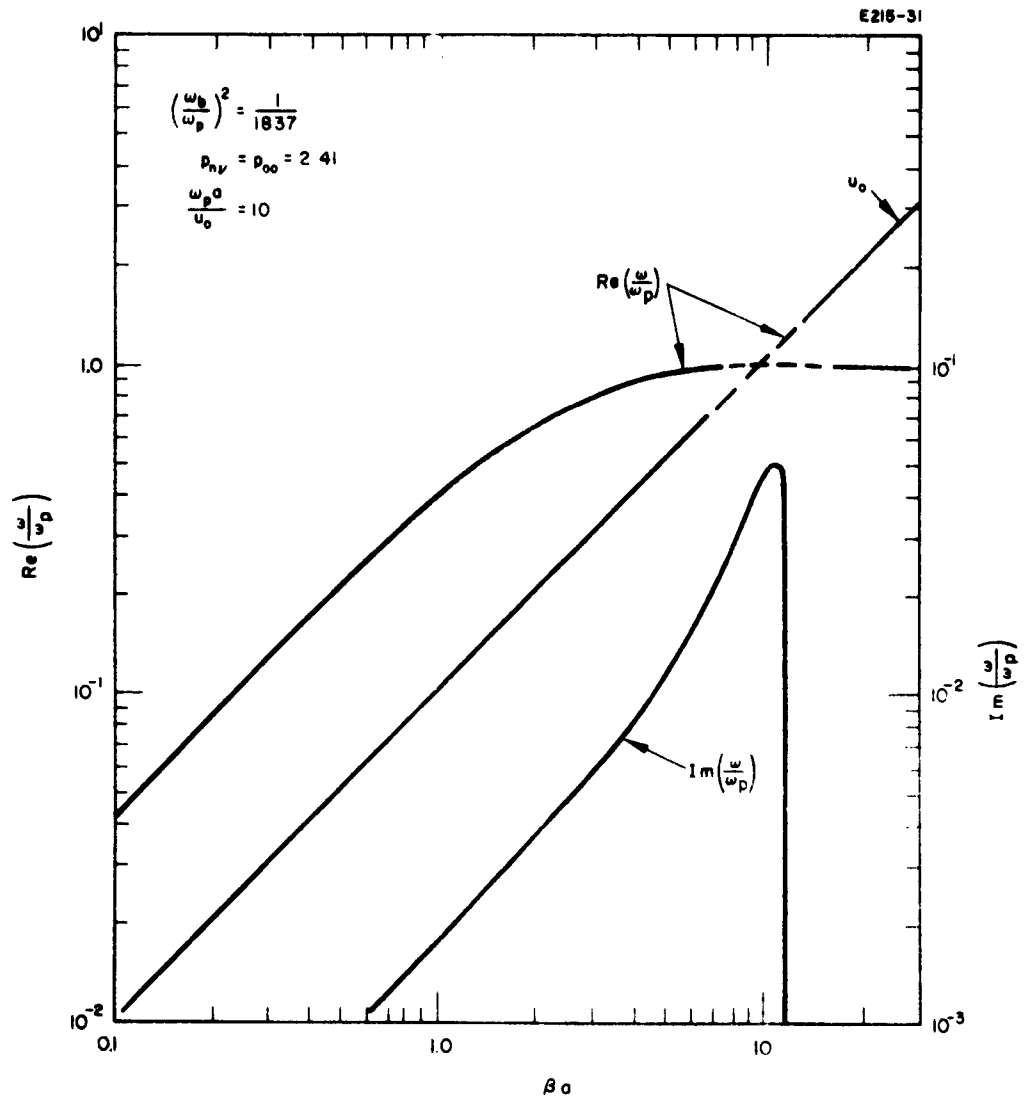


Fig. 16. Expanded dispersion diagram for the symmetrical mode of a plasma column.

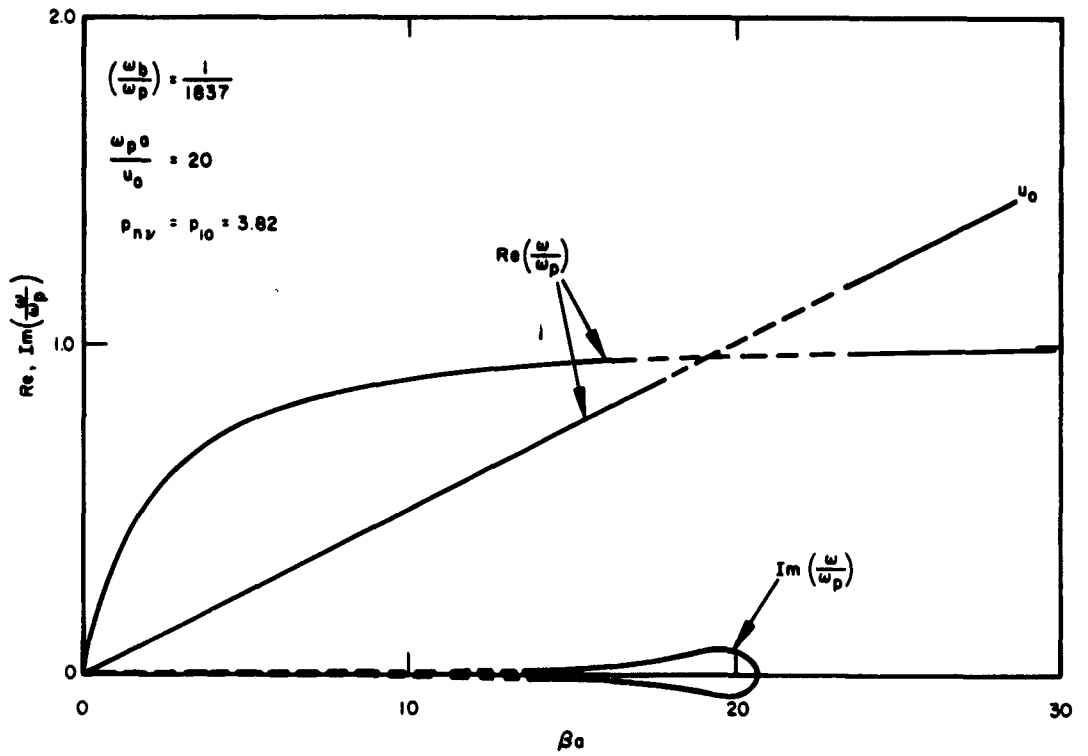


Fig. 17. Typical dispersion diagram for the mode of one angular variation of a plasma column with injected electrons.

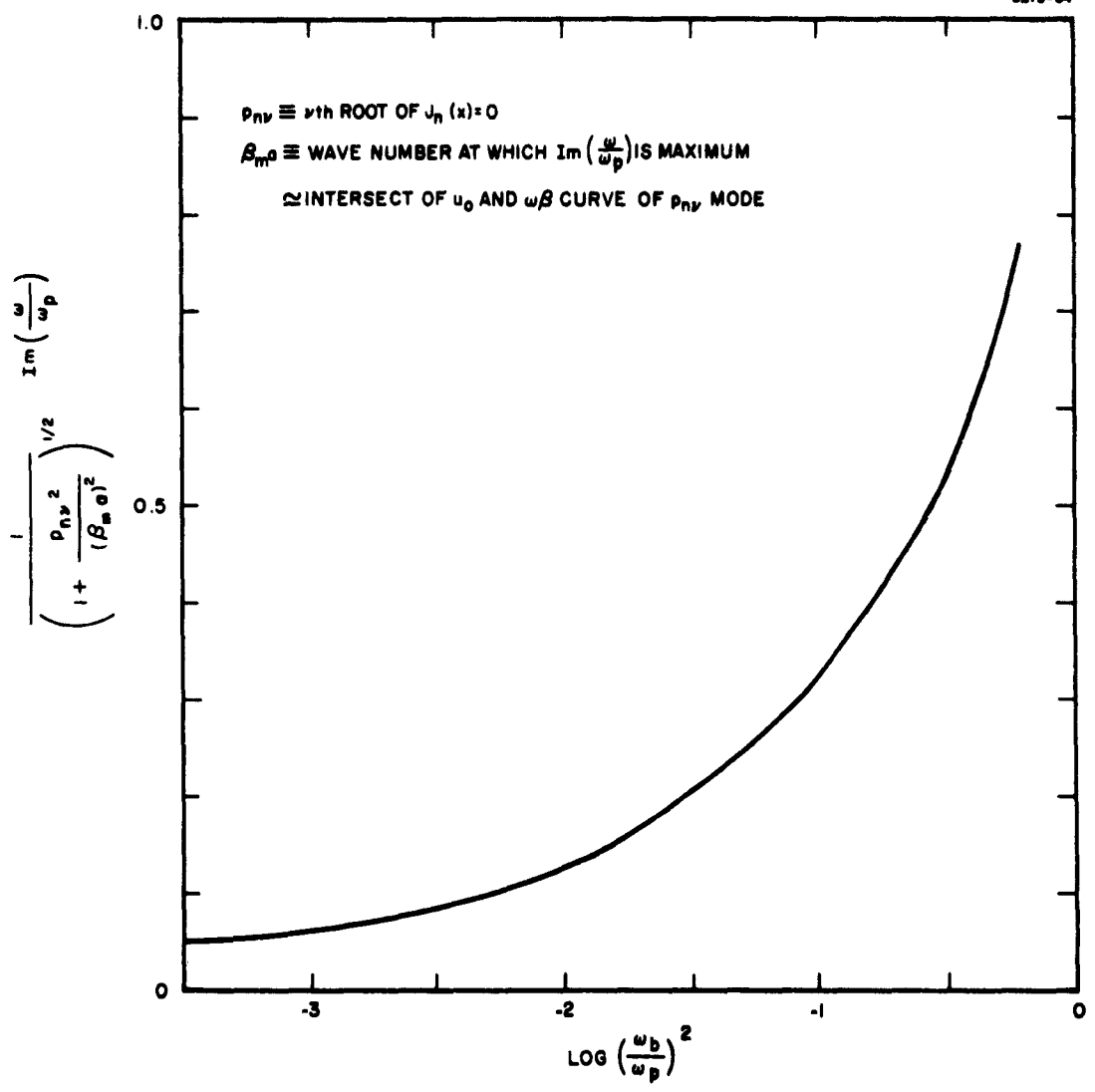


Fig. 18. The dependence of the maximum growth rate of instability as a function of (ω_b/ω_p) .

It should be remarked that the foregoing calculations are based on the dispersion equation (eq. 14). This dispersion equation was derived¹³ under the assumption that the plasma column completely fills the inside of the conductor. In fact, conditions found in our experiment differ considerably from this model. The conductor to the plasma column diameter ratio is on the order of 10. The effect of such an increase is found mostly for small values of βa or ω/ω_p , as shown in Fig. 19. The maximum phase velocity becomes larger as b/a is increased. This condition should, therefore, increase the range of u_0 for which the intersection of the ω - β curve and the u_0 line is possible.

The theory developed to this point shows that growing waves amplifying perturbations of the electrons injected into a collisionless plasma column can exist under the conditions of our experiments. The existence of such instabilities is necessary, but it is not sufficient for the thermalization of the fast injected electrons. We need to demonstrate that these instabilities, predicted on the basis of a linearized theory, do lead to a large amplitude nonlinear limit. We now must establish that the instability growth rate is sufficiently large that a perturbation in velocity grows to a magnitude of the order of the injection velocity of the injected electrons.

4. Thermalization Through Large Signal Effects

a. Bunemans's Condition for Nonlinear Thermalization — In the preceding section we have shown that the presence of injected electrons gives rise to a growing instability. We shall examine whether the nonlinear limit can be achieved in our electron injection experiments. The approximate criterion which is to be applied here was derived by Buneman⁸ and has the following form:

$$\frac{\text{Fluctuation Energy}}{\text{Drift Energy}} = \frac{1}{9f_p} \left(\frac{l}{\lambda_p} \right)^3 \left(\frac{6\pi a_m}{t} \right)^{1/2} e^{2a_m t} \quad (15)$$

where

$$a_m = \text{Im} \left(\frac{\omega}{\omega_p} \right)$$

$f_p \equiv$ plasma frequency

$l \equiv n^{-1/3}$ mesh size, if electrons were arranged in a cubic lattice.

$\lambda_p = \frac{u_0}{f_p} \equiv$ distance traversed by electrons in one plasma period.

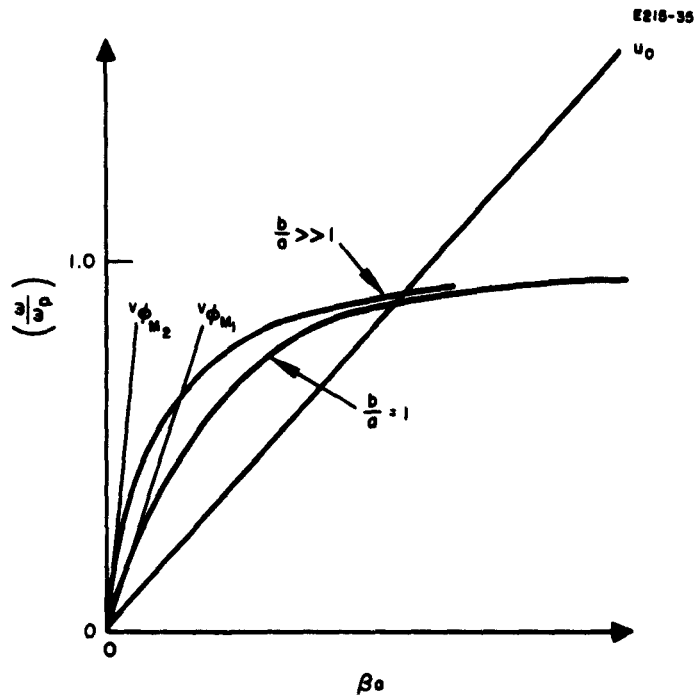


Fig. 19. The behavior of the dispersion diagram for an electrostatic plasma wave mode as a function of the dimensions of the surrounding conductor.

The time or distance required for the fluctuation energy to be amplified and to reach the drift energy can be estimated from (15) by setting (15) equal to unity.

Typical values for the parameters of (15) corresponding to our experimental conditions follow: $f_p = 2.8 \times 10^8$ cps; $l = 10^{-3}$ cm; $u_o = 4.2 \times 10^8$ cm/sec at $\mu_o^2/2P = 50$ eV; $\lambda_p = u_o/f_p = 1.5$ cm. The growth rate α can be estimated by using Fig. 18 for $(\omega_b/\omega_p)^2 = 1/100$; the conservative estimate of $\alpha_m = 0.12 \omega_p$ is obtained. The random energy becomes equal to that of the drift energy when $f_{pt} \cong 15$, i. e., in 15 plasma periods.

We now compute the time required for injected electrons to travel from the electron emitter to the plasma emitter. The distance is $L \cong 30$ cm. Thus, $Tf_p = (L/u_o) f_p \cong 20$ periods. The injected electrons, therefore, require about 20 plasma periods before they reach the plasma emitter. At least, Buneman's criterion for the randomization of the injected electrons is not violated. This alone, however, is not conclusive, since Buneman's criterion is only approximate. The possibility for enhanced instability growth by instability "trapping," as discussed below, is therefore of importance.

b. Instability "Trapping"— Upon examination of the boundary conditions, however, the transit time of 20 plasma periods becomes more favorable as the condition required for the nonlinear randomization of the injected electrons is naturally satisfied. The plasma emitter and the electron emitter located at the two ends of the plasma column can be considered as two reflecting plates for the plasma waves. Hence any growing instability will essentially be "trapped" between these two plates and in due time can reach a large-amplitude nonlinear limit. This "trapping" of an instability can be explained as follows: When a small fluctuation (e. g., of thermal origin) appears at a point in the plasma column such as the accelerating sheath near the electron emitter, this disturbance will grow as it travels in the direction of the drifting electrons according to the rate determined from the dispersion equation of the system. Upon reaching the end of the plasma column, the plasma wave associated with the original fluctuation will be reflected back from the plasma boundary (plasma emitter). As such a wave propagates in the back direction, no interaction with the streaming electrons will occur. In the absence of excessive losses, the returned wave will be re-reflected at the electron emitter surface. At this time, it is no longer at the same thermal energy level as the original fluctuation. It will modulate the injected electron stream and be further amplified until it again reaches the plasma emitter end, and so on. It is possible, then, that even a slowly growing wave could reach a large-amplitude nonlinear limit after making several reflections and could contribute to the thermalization of the injected electrons.

It was shown in Fig. 16 that the growing instability existed for all frequencies smaller than the plasma frequency ($\omega \leq \omega_p$) although the rate of growth decreased rapidly as a decreasing function of βa . For $\text{Re} \omega \cong \omega_p$, the rate of growth has a maximum value $\text{Im}(\omega/\omega_p) \cong 0.05$ for $(\omega_b/\omega_p)^2 = 1/1833$ and $\omega_{pa}/u_0 = 10$. On the other hand, $\text{Im}(\omega/\omega_p) \cong 0.002$ or at $\text{Re}(\omega/\omega_p) \cong 0.10$. Thus, if instability trapping did not occur, noise components at higher frequencies would have a much larger amplitude than those at lower frequencies. In the presence of instability trapping and with higher order modes in synchronism with even relatively slow injected electrons, this is, however, not necessarily the case. This will be shown by the noise spectra measurements reported in the next sections.

C. Noise Spectrum Measurements

1. Experimental Apparatus and Experimental Conditions

The measurements of the noise radiation spectrum have been performed using a cesium plasma generator with an injection cathode as shown in Fig. 20. This apparatus is similar to that of Fig. 1, whose operation was described in Section III.

For the purposes of the present experiments, two coaxial probes were installed in the apparatus, as shown in Fig. 20. The center conductor of one of the coaxial probes utilized the thin wire which was originally used as a Langmuir probe and was connected across the glass envelope through the plasma column. The other coaxial probe was made of a standard 50Ω rigid coaxial line and was placed approximately 3 cm radially away from the plasma column. The oscillation spectrum inside the plasma column and outside of it was obtained from these coaxial probes, using commercial spectrum analyzers (Panoramic Model SPA-4A and Panoramic Model SPA-3). The SPA-4A spectrum analyzer was used at all frequencies from 6 Mc up to 10 Gc, whereas the latter analyzer was used from 200 cps up to 12 Mc.

The plasma density and the plasma electron temperature were measured with a cylindrical Langmuir probe located 3.5 cm away from the plasma emitter. The movable probe as shown in the Fig. 20 was used only as a mode suppressing floating probe whose function will be described in more detail later. Experiments were conducted over a wide range of injection conditions at plasma densities on the order of 10^9 electrons/cm³. These conditions correspond to those under which the probe measurements of the plasma electron temperature and the estimate of the degree of randomization of the fast electrons in a collisionless plasma have been made (see Section IV-C).

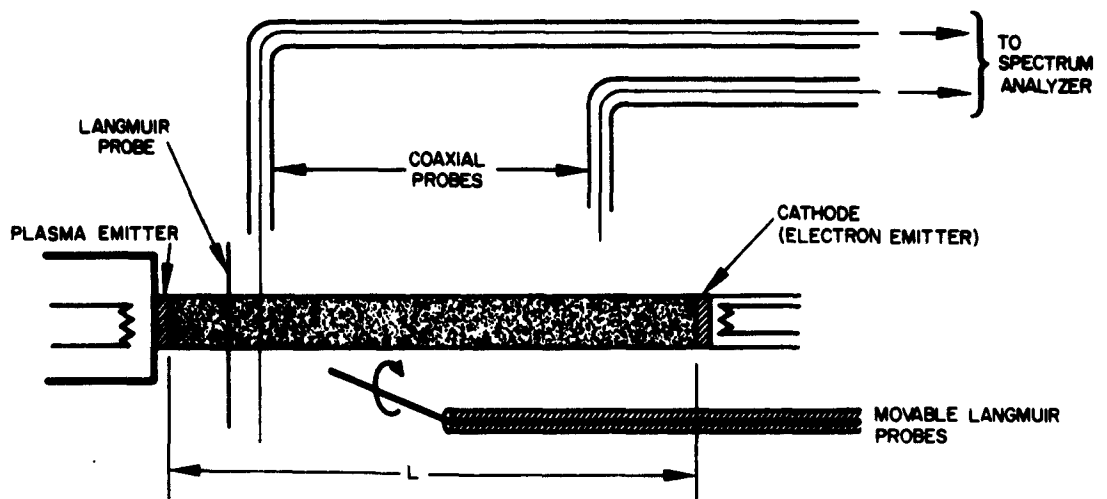


Fig. 20. Cesium plasma generator instrumented with electron emitter, coaxial probes, and movable Langmuir probe for the measurement of the noise spectrum as a function of injection condition.

The experimental conditions were as follows:

Plasma Density	$n_p = 10^9 \text{ electrons/cm}^3$
Plasma Frequency	$f_p = 280 \text{ Mc}$
Injected Electron Density	$n_b = (1/100)n_p$
Injected Electron Plasma Frequency	$(\omega_b/\omega_p)^2 = 1/100$
Injection Energy	$0 < \mu u_o^2/2 < 50 \text{ eV}$
Plasma Column	
Length	$L = 29 \text{ cm}$
Diameter	$2a = 1.27 \text{ cm}$
Injected Electrons	
Diameter	$2a = 1.27 \text{ cm}$
Outer Conductor (rf Shield)	$2b = 14 \text{ cm}$
Magnetic Field	$B_o = 1500 \text{ G}$
	$\omega_c/\omega_p \geq 14$
Initial Plasma Temperature	$T_e = 0.2 \text{ eV}$

2. Noise Spectrum Observed with a Coaxial Probe Immersed in the Plasma

Noise spectra have been measured using probes in and out of the plasma column as shown in Fig. 20 in the presence of injection of fast electrons from the injection cathode. These measurements yielded the spectra shown in Fig. 21(a) and 21(b). With the probe located outside, the oscillation spectrum was observable only at low frequencies. (We shall describe the nature of this "outside" spectrum in more detail later.) The noise level inside the plasma column, on the other hand, covered a wide range of frequencies, extending from a few megacycles up to at least the electron plasma frequency f_p . The upper limit of these noise spectra could not be determined with confidence because of a lack of receiver sensitivity. Some irregular variations and a gradual decrease of the amplitude of oscillation have been observed. These variations are believed caused by the nonflat response of the spectrum analyzer and by some impedance mismatch expected to exist at the coaxial probes.

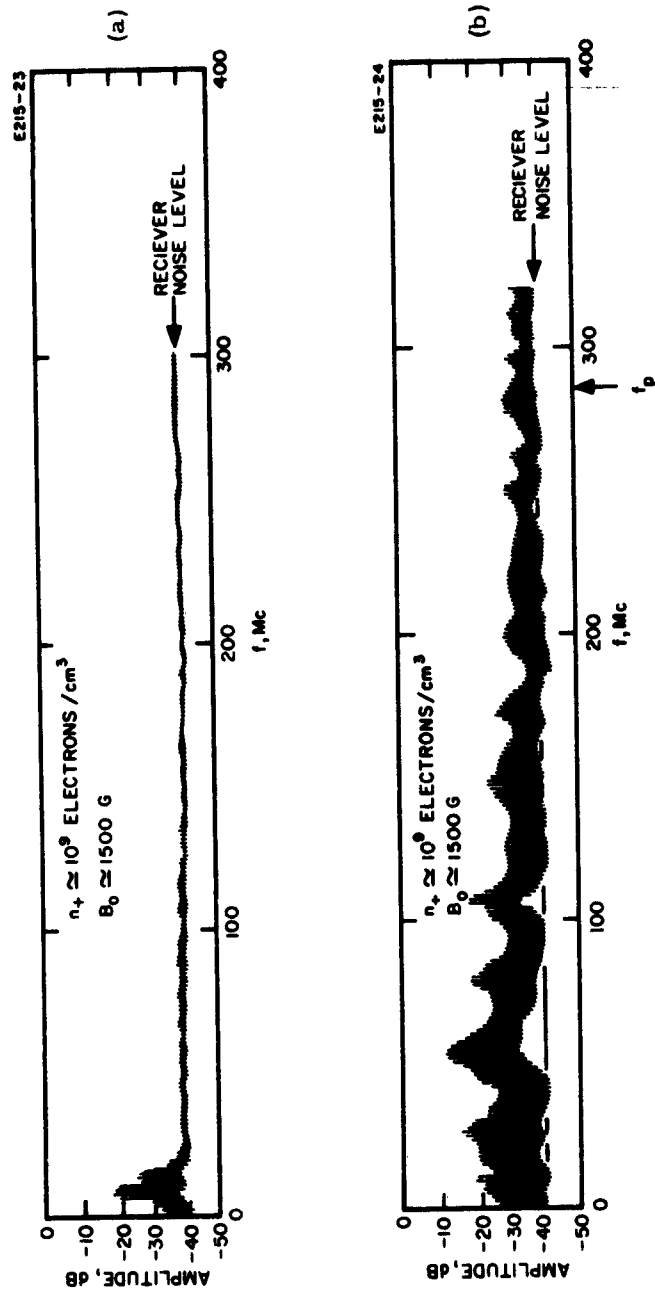


Fig. 21. The measured noise spectrum (in presence of injected electrons) as a function of frequency. (a) Measured with a coaxial probe outside plasma column. (b) Measured inside the plasma.

Changes of injection conditions, plasma density, and dc magnetic field over relatively large ranges did not affect the general aspect of the noise spectrum. Noise was always generated over the entire range up to frequencies at least of the order of the plasma frequency, with amplitudes which did not seem to vary greatly over this frequency range.

These observations are consistent with the theory of electron-plasma wave interaction which was shown in Section B to predict the possible existence of enhanced fluctuations (noise) at all frequencies up to the plasma frequency, the lower frequency noise in particular being enhanced by instability trapping.

3. The Noise Spectrum Observed Outside the Plasma Column

It was indicated earlier that noise outside of the plasma column was observable only at low frequencies (See Fig. 21(a)). In detailed investigations made later, this noise spectrum measured outside of the plasma column exhibited very interesting and revealing characteristics which will now be reported.

a. Typical Spectrum-Resonance Modes — A noise spectrum observed outside the plasma column is shown in Figs. 22(a), 22(b) and 23. The actual unfiltered spectrum is shown in Fig. 22(a) and is sketched over a wider frequency range in Fig. 23. Peaks as shown in these figures are relatively well defined. They are found to correspond to axial resonances of the growing waves predicted from the dispersion equation (eq. (18)). Growing waves have been shown to exist for $\omega/\omega_p \approx 1$. The real part of the frequency is given approximately by the synchronism condition:

$$\beta u_o \approx \text{Re}(\omega) . \quad (16)$$

Thus, in terms of the wavelength $\beta = 2\pi/\lambda$, we have

$$\text{Re}(\omega) = \frac{2\pi u_o}{\lambda} . \quad (17)$$

The resonance modes are found for frequencies such that the separation of the conducting end plates is an integral number of half a wavelength. Equation (17) accounts for these three resonances:

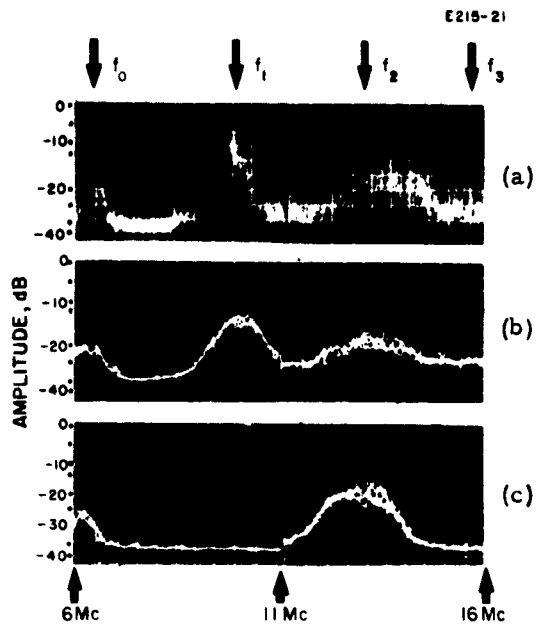


Fig. 22. The noise spectrum at low frequency limit obtained with a coaxial probe outside the plasma. (a) Unfiltered spectrum; full oscillation. (b) Filtered spectrum; full oscillation. (c) Filtered spectrum; partially suppressed oscillation.

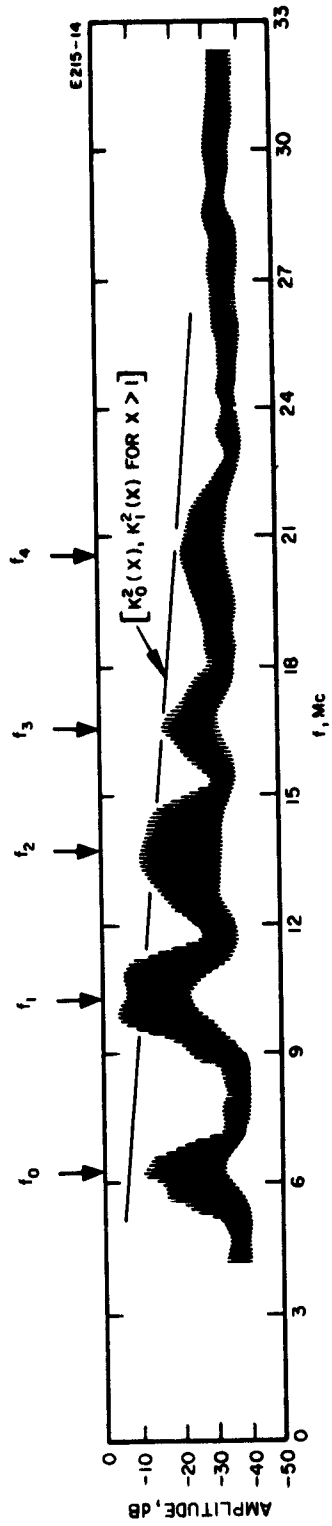


Fig. 23. Typical peaks of the low frequency noise spectrum observed outside the plasma column.

	$f_0, \text{ Mc}$	$f_2, \text{ Mc}$	$f_4, \text{ Mc}$
Experiment	6.4	13.5	19.5
Theory	6.5	13	19.5

These are associated with the symmetrical mode, whereas f_1 and f_3 are associated with the $n = 1$ angular variation mode. The latter two have not quantitatively been explained. The symmetrical modes f_0 , f_2 , and f_4 show good agreement with the theory (eq. (17)) for $30 < V_0 < 140 \text{ V}$, where V_0 is taken practically equal to the injection voltage. Observation of these "resonance" peaks in the noise spectrum lends strong support to the theory of "instability trapping" by multiple reflections of the plasma waves at the ends of the plasma column.

The width of the peaks demonstrates an interesting behavior. For a given injection voltage, the amplitude of the peaks was not affected by changing the injection current density. The width of each peak, however, became narrower as the current density was decreased while keeping the injection voltage constant; the width increased as the plasma temperature increased. It appeared that the nonlinear limit or the saturation condition was achieved even at low injection current densities.

b. Relative Amplitude of Resonant Modes — The spectral distribution observed with a probe immersed in the plasma had indicated similar peaks; unlike those shown in Fig. 23, the magnitude of the peaks remained approximately equal while the valleys between the peaks were a decreasing function of frequency. Assuming then that the magnitude of the peaks inside the plasma were mutually equal, we could estimate the function dependence of the peaks observed outside the plasma. Upon examining the field equation (eq. (11)) and noting that the location of the probe was about $r_0 = 3 \text{ cm}$ whereas $b = 7 \text{ cm}$, we could show that for $r_0 = 3 \text{ cm}$

$$E_z \propto K_n(\beta r_0)$$

where

$$\beta = \frac{2\pi}{\lambda} \propto \omega .$$

Thus, βr_0 is a linearly increasing function of ω . Using a large argument approximation, $K_0^2(x)$ and $K_1^2(x)$ functional dependences are shown in Fig. 23. The curve is scaled to indicate the relative values of the observed peaks of the resonant mode. Agreement seems quite reasonable.

c. Partial Suppression of the Oscillation and its Effect on the Probe I-V Characteristics — One of the significant observations made during the spectral measurement of the noise radiation from the cesium plasma experiments was that the $n = 1$ modes (one-angular variation) could be suppressed by placing a set of floating Langmuir probes radially at the center of the plasma column. The composite photographs shown in Fig. 22 (c) clearly demonstrate the suppression of every other mode. The suppressed modes are believed to be associated with the $n = 1$ resonant mode. The probe position for suppressing these modes was in general found very critical. As the probes approached the center of the plasma column (as shown in Fig. 24), a sudden disappearance of the $n = 1$ mode was accompanied by a small increase in the amplitude of the adjacent peaks. A comparison between (b) and (c) of Fig. 22 shows that near complete suppression was obtained.

Langmuir probe I-V characteristics were obtained simultaneously with these spectral measurements. While the movable probe was outside the plasma column, the probe characteristic indicated a smooth variation. As soon as the floating movable probes were used to suppress a portion of the noise peaks, the probe characteristic noticeably changed: a step in the probe characteristic appeared at the potential near the injection potential of electrons (Fig. 25). This shows that as part of the noise spectrum was suppressed, an appreciable number of injected electrons retained their initial injection energy. This is consistent with the theoretical expectation that when a number of the possible modes of electron-plasma interactions which contribute to the thermalization of fast electrons are suppressed by these probes, the rate of energy transfer from the fast electrons to the slow electrons in the plasma is reduced. This significant change in the probe characteristic with the noise spectrum is a direct demonstration of the importance of the electron-plasma wave interaction discussed above for the thermalization of the fast injected electrons.

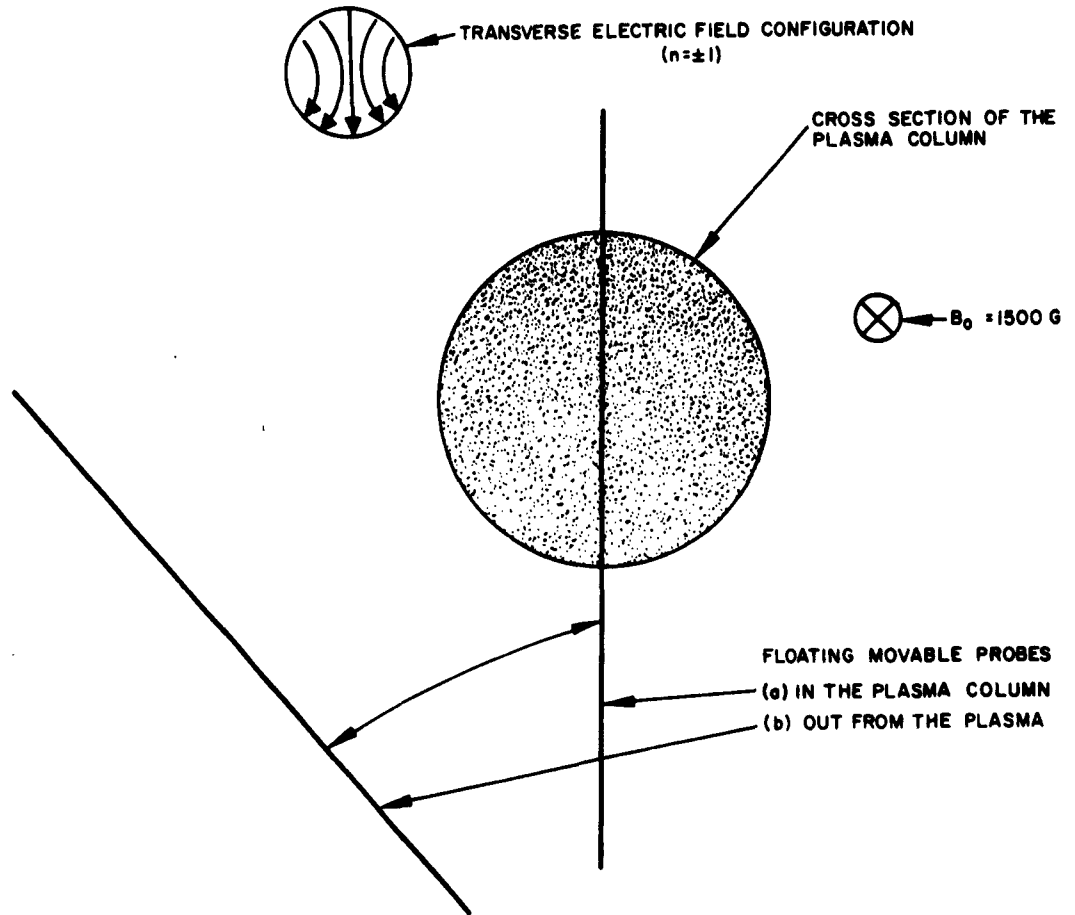


Fig. 24. A schematic diagram of the floating movable probes used for partial suppression of the noise in a plasma.

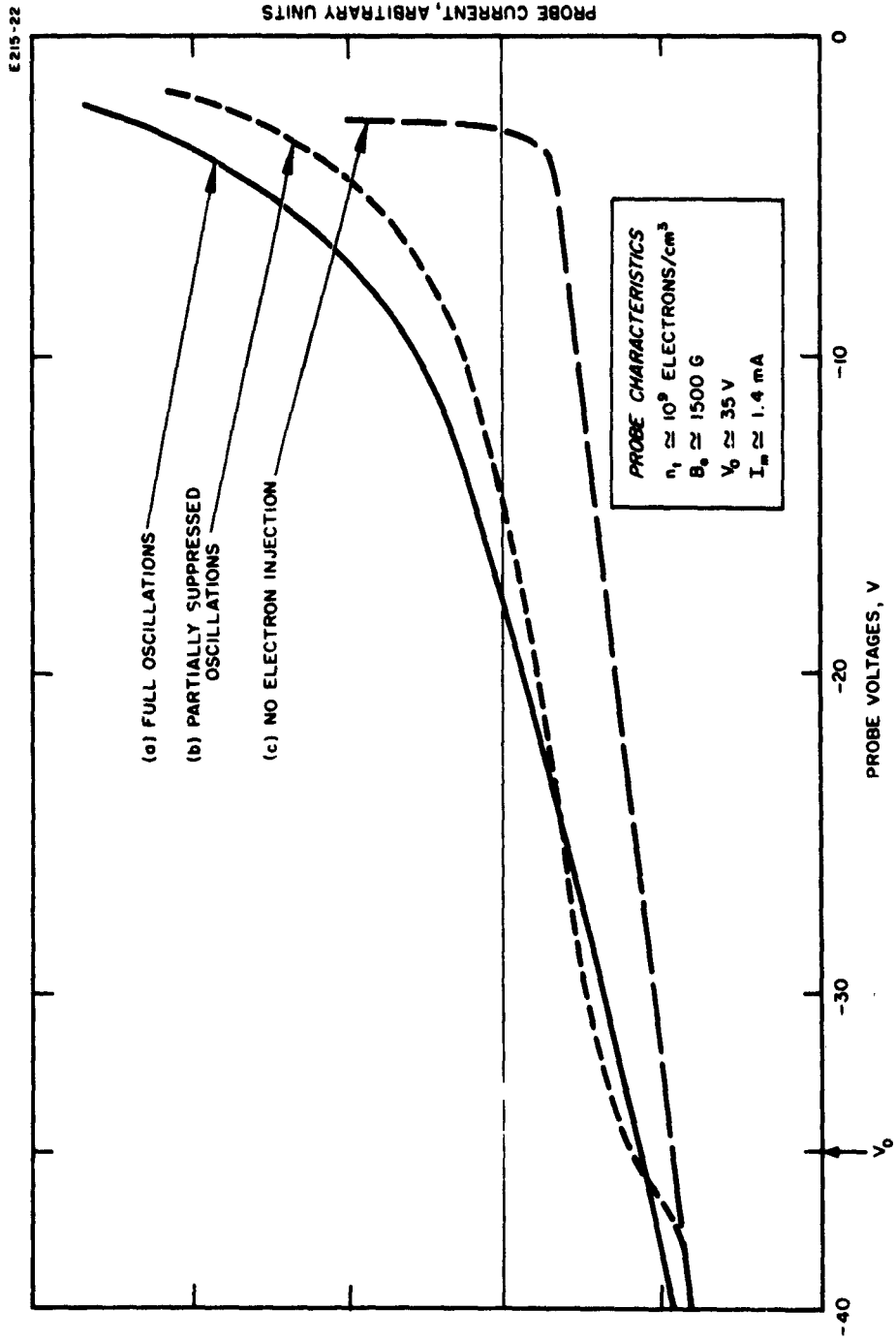


Fig. 25. Effect of partial suppression of the oscillation on Langmuir probe I-V characteristics.

VI. ELECTRICAL RESISTIVITY OF A HIGHLY IONIZED CESIUM PLASMA

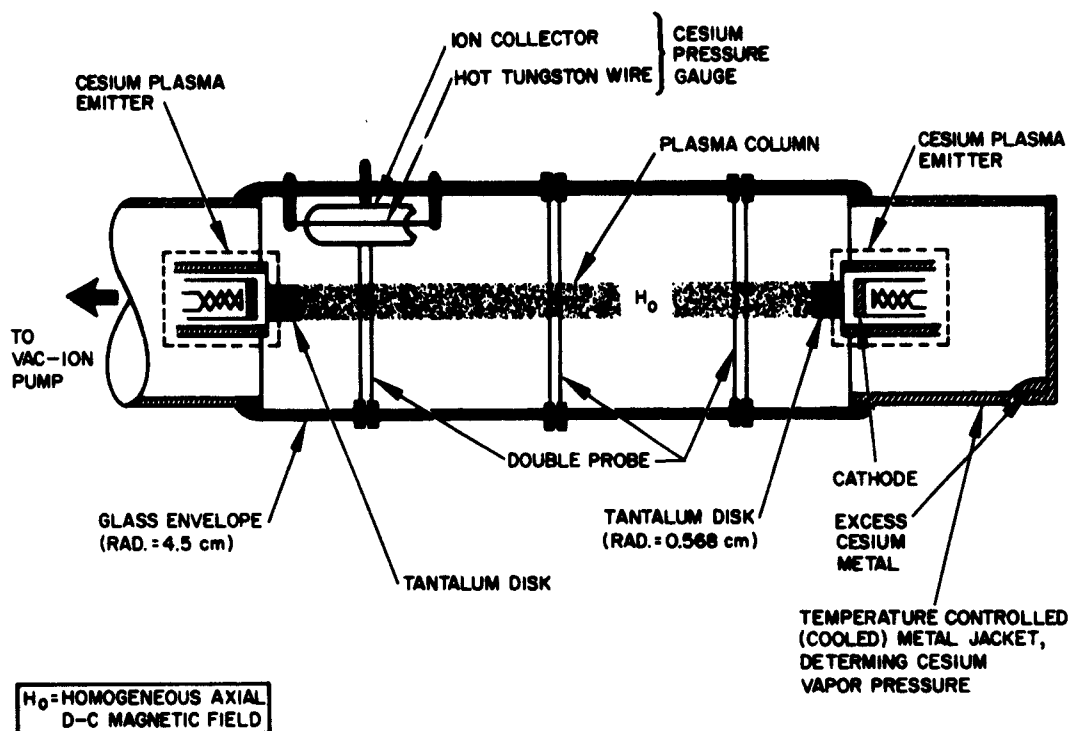
A. Method of Measurement

The resistivity of a highly ionized quiescent plasma is to be measured and compared with the theoretically determined value. A highly ionized plasma is understood here to mean a plasma in which Coulomb collisions are predominant and electron neutral collisions negligible. A quiescent plasma is understood to be a plasma in which electrons and ions have Maxwellian velocity distributions. Such a highly ionized quiescent plasma is produced by a cesium plasma tube with two plasma emitters, similar to that already developed and used during Phase I of this contract for the study of volume recombination. The tube used for the plasma resistivity measurement is shown in Fig. 26. The thermal cesium plasma is generated at two hot tantalum emitters which are separated by 30 cm; this plasma is confined magnetically to a well-defined diameter approximately equal to that of the tantalum emitter disk (1.27 cm diameter). Since the electron motion is confined mainly to the line of force of the magnetic field, the measurement and the interpretation of the resistivity is simply a one-dimensional problem. The tube also has three sets of double probes for plasma density and temperature measurements.

The dc or low-frequency resistivity of the plasma can be measured by two methods. One method utilizes probes to measure the potential difference between two given locations in the presence of a small current flow through the plasma column. With the other method, which is more reliable, the resistivity is obtained from the slope of the I-V characteristic between the two plasma emitters of the tube.

The use of probes at different locations to measure the potential drop in a current-carrying plasma column has been used to some extent in the measurement of plasma resistivity. However, uncertainty in the work function of the probes and in their floating potential with respect to the plasma makes this method rather unreliable.

The use of the I-V characteristic between the two plasma emitters for the measurement of the resistivity at first examination appears more complicated because of the presence of the space charge sheaths near the emitter surfaces. The effect of the space charge sheath, however, is amenable to analysis and can be made smaller compared with that of the volume resistivity by properly controlling the plasma parameters. By this method, furthermore, the resistivity is measured for low current densities, where ohmic heating is negligible. In order to apply this method of measurement reliably, we shall now analyze the respective effects of the emitter sheaths and of the plasma resistivity on the I-V characteristics between the two plasma emitters.



- NOTES:
1. ATMOSPHERE: Cs VAPOR, AT PRESSURE BETWEEN 1 AND 10^{-6} mm Hg APPROX.
 2. VAC-ION PUMP USED ONLY FOR PROCESSING. IT IS TURNED OFF DURING EXPERIMENT.
 3. LENGTH OF THE PLASMA COLUMN IS 30 cm.

Fig. 26. Probe instrumented cesium plasma tube with two plasma emitters.

B. Current-Voltage Characteristics between Plasma Emitters

The first treatment of the sheath effect for a double emitter system was given by D'Angelo and Motley.¹⁵ Their derivation was restricted to the case where the emitter temperature was sufficiently high that negative space charge sheaths were formed near the emitter surfaces, the plasma potential being negative with respect to the vacuum potential of the emitters. We are extending the analysis also to the case in which positive sheaths are formed, and are using a method of analysis which is simpler than that of D'Angelo and Motley.

The axial potential distributions in the presence of a small applied potential difference between two emitters are shown in Figs. 27(a) and 27(b). As shown in these diagrams, the sheath thickness is much smaller than the separation between the two emitters. V_1 and V_2 are the sheath potentials associated with emitters No. 1 and 2, respectively. The top distribution (Fig. 27(a)) corresponds to the case in which negative space charge sheaths are formed, whereas in Fig. 27(b) the positive sheaths are formed. The current is drawn from one emitter to the other when a voltage V is applied between the two emitters. With the application of a strong dc magnetic field, the current flow will be essentially one dimensional, and the cross section of the current carrying plasma can be assumed equal to the emitter area. The resistive drop across the plasma due to the current flow is given in Figs. 27(a) and 27(b) by V_3 , which is related to the resistivity through the following familiar expression

$$V_3 = I \frac{\eta L}{A} \quad (18)$$

where η is the resistivity of the plasma, L is the length of plasma columns, and A is the cross sectional area of the plasma emitter and the plasma carrying the current I . The similarities between the two cases end at this point. We must now treat each case separately. We will consider the negative sheath case first. In this analysis, we shall assume that the electron losses in the plasma column due to the volume recombination and due to transverse diffusion are negligible. These assumptions do not seriously affect the analysis—inclusion of these electron losses only slightly changes the condition for the transition from one type of space charge sheath to the other.

1. Theory of the Negative Space Charge Sheath Case ($j_{sat-} > j_{p-}$)

The condition necessary to form a negative space charge sheath is that the saturation thermionic emission current (j_{sat-}) be larger than the random plasma electron current reaching the emitters [$j_{p-} = en(\bar{v}_e/4)$]. n is defined as the plasma density and \bar{v}_e is the average thermal velocity of electrons in the plasma. Using these notations, the relationship between various currents and voltages can be written as follows:

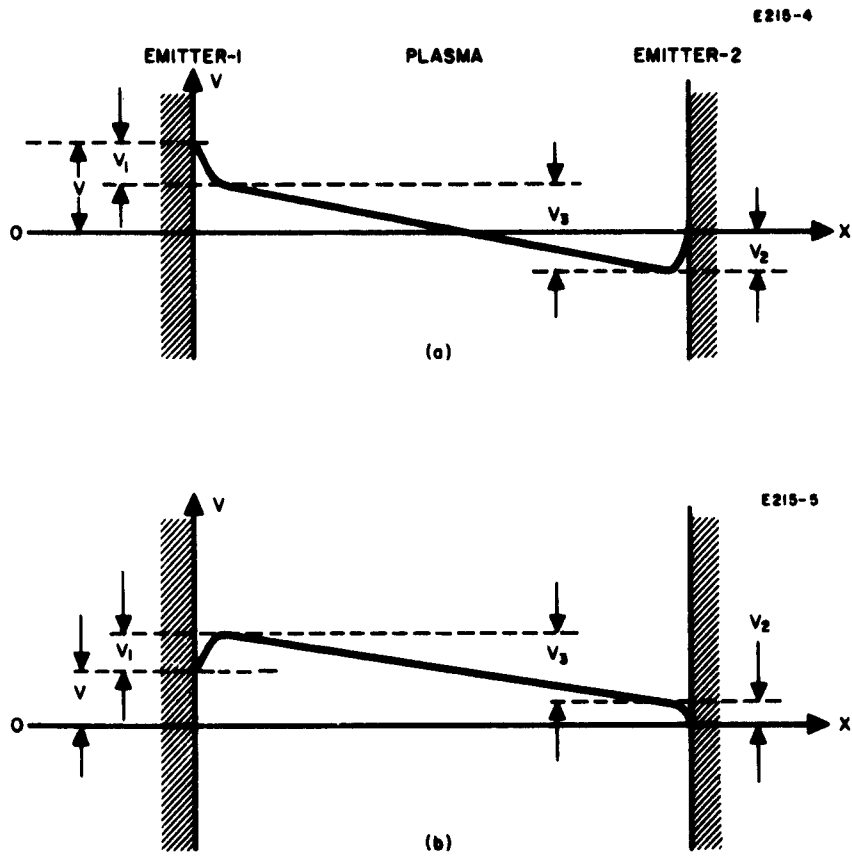


Fig. 27. Typical axial potential distribution for biased plasma emitters. (a) Negative space charge sheath case. (b) Positive sheath case.

At Emitter No. 1

$$I = A_{j_{p-}} - A_{j_{sat-}} \exp(-eV_1/kT) . \quad (19)$$

At Emitter No. 2

$$I = A_{j_{sat-}} \exp(-eV_2/kT) - A_{j_{p-}} , \quad (20)$$

whereas

$$V = V_1 + V_3 - V_2 \quad (21)$$

where

$k \equiv$ Boltzmann constant

$T \equiv$ the plasma temperature which is equal to the emitter temperature for $I \ll A_{j_{p-}}$.

As was shown, V_3 is related to I through (18). After combining (18), (19), (20), and (21) and eliminating j_{sat-} , V_1 , V_2 , and V_3 , the above expressions reduce to one equation

$$V = \frac{\eta L}{A} + \frac{kT}{e} \left[\ln(A_{j_{p-}} + I) - \ln(A_{j_{p-}} - I) \right] . \quad (22)$$

Next, we take the derivative with respect to I . The random plasma current density j_{p-} can be considered constant for a small variation of either V or I (which has been verified experimentally in a two-emitter system). By taking the derivative for $I \rightarrow 0$ we obtain:

$$\lim_{I \rightarrow 0} \frac{dV}{dI} = \frac{\eta L}{A} + \lim_{I \rightarrow 0} \frac{kT}{e} \left(\frac{1}{A_{j_{p-}} + I} + \frac{1}{A_{j_{p-}} - I} \right)$$

or

$$\left. \frac{dV}{dI} \right|_{I \rightarrow 0} = \frac{\eta L}{A} + \frac{2kT}{eA_{j_{p-}}} = \frac{\eta L}{A} + \frac{2kT_e}{eA \left(\frac{en - \bar{v}_-}{4} \right)} \quad (23)$$

which is identical to D'Angelo's and Motley's but derived somewhat differently here.

Inspection of the above expression shows that the effect of the sheath voltages predominates at low densities:

$$\lim_{\substack{n \rightarrow 0 \\ I \rightarrow 0}} \frac{dv}{dI} = \frac{8kT_e}{e^2 A n_- \bar{v}_-} \quad (24)$$

For higher plasma densities, the ohmic voltage drop becomes predominant and, for a relatively large density so that

$$\frac{2kT}{e\eta L j_{p-}} \ll 1,$$

the plasma resistivity is accurately obtainable by means of (23).

2. Theory of the Positive Space Charge Sheath Case ($j_{sat-} < j_{p-}$)

The condition required for this case is that ($j_{sat-} < j_{p-}$). The procedure used for the positive space charge sheath is similar to that for the negative sheath. We write the current-voltage relations for the two emitters:

At Emitter No. 1

$$I = A \left[j_{p-} \exp\left(\frac{-eV_1}{kT}\right) - j_{sat-} \right] \quad (25)$$

At Emitter No. 2

$$I = A \left[j_{sat-} - j_{p-} \exp\left(\frac{-eV_2}{kT}\right) \right] \quad (26)$$

and for voltages

$$V = V_2 + V_3 - V_1 \quad (27)$$

Combining these equations with (18), we are left with an equation which relates the applied voltage to the conduction current:

$$V = \frac{\eta L}{A} + \frac{kT}{e} \left[\ln(Aj_{\text{sat-}} + I) - \ln(Aj_{\text{sat-}} - I) \right]. \quad (28)$$

Evaluating the slope of the I-V characteristic for $I \rightarrow 0$, we get an expression similar to (23):

$$\left. \frac{dV}{dI} \right|_{I=0} = \frac{\eta L}{A} + \frac{2kT}{eAj_{\text{sat-}}} \quad (29)$$

Note that when $j_{\text{sat-}}$ is replaced with j_{p-} , eq. (29) transforms to (23). The physical meaning is the following: For a given cesium plasma density, it is possible to increase the emitter temperature above a certain minimum value without greatly affecting the plasma density. Therefore, for a given density, the contribution of the sheath voltage drops may be minimized by increasing the electron emission rate. However, the further increase of $j_{\text{sat-}}$ beyond $j_{\text{sat-}} > j_{p-}$ has no noticeable effect.

3. Comparison of Experimental I-V Characteristics with Theory

Examination of the emitter temperature (and thus $j_{\text{sat-}}$) and of the plasma density (or j_{p-}) prevalent in our experiments shows that $j_{\text{sat-}} < j_{p-}$; hence (29) is applicable for our experimental conditions. The experimental points obtained from I-V characteristics such as the one shown in Fig. 28 under these conditions are plotted in Fig. 29 and compared with the theoretical values calculated by using (29) and Spitzer's equation for η :

$$\eta = 6.53 \times 10^3 \frac{\ln \Lambda}{T^{3/2}} \Omega \text{-cm} \quad (30)$$

The numerical values of the function $\ln \Lambda$ are tabulated and given by Spitzer,¹⁶ whereas the second term of the RHS of (29) is calculated from the optically measured temperatures of plasma emitters and $j_{\text{sat-}}$ estimated from the thermionic electron emission characteristics of pure tantalum metal. The experimental points were obtained with the two-emitter Cs^+ plasma tube shown in Fig. 26 and described earlier in Section VIA. As observed in Fig. 29, the calculated theoretical values are consistently larger than the measured values; the general distribution of the experimental points shows that the sheath effects predicted by (29) are quantitatively in agreement with the experimental results. It is further observed that for low plasma densities sheath effects become much greater than the effect of volume resistivity; reliable measurements of volume resistivity by this method should therefore be made at higher densities where the contribution due to the sheath potential is much smaller than that of the volume resistivity.

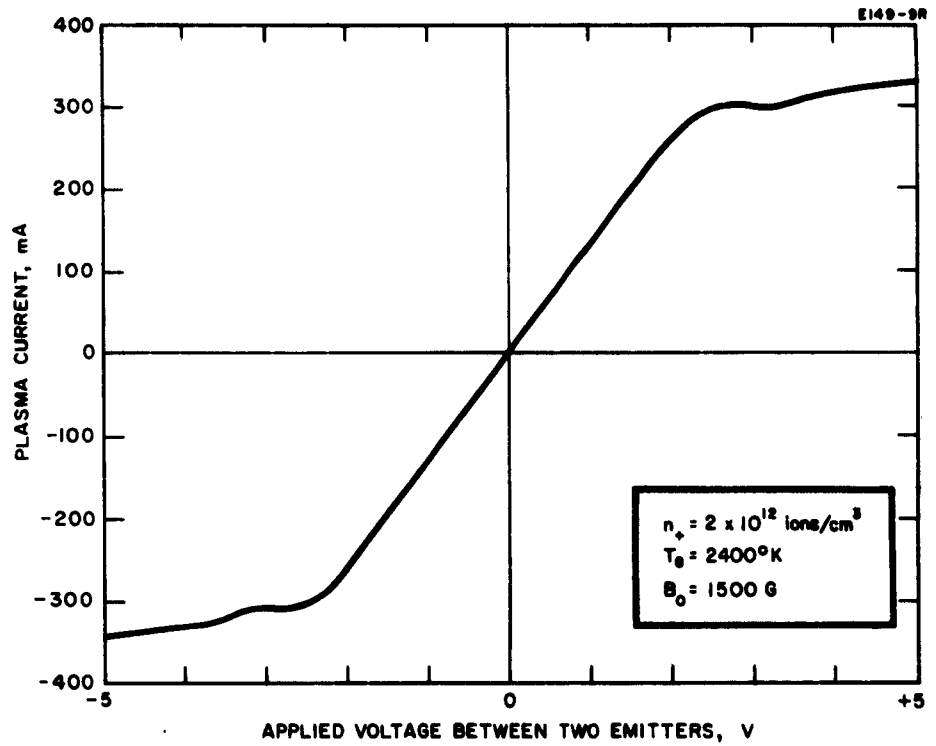


Fig. 28. Typical I-V characteristics of the cesium plasma tube with two plasma emitters.

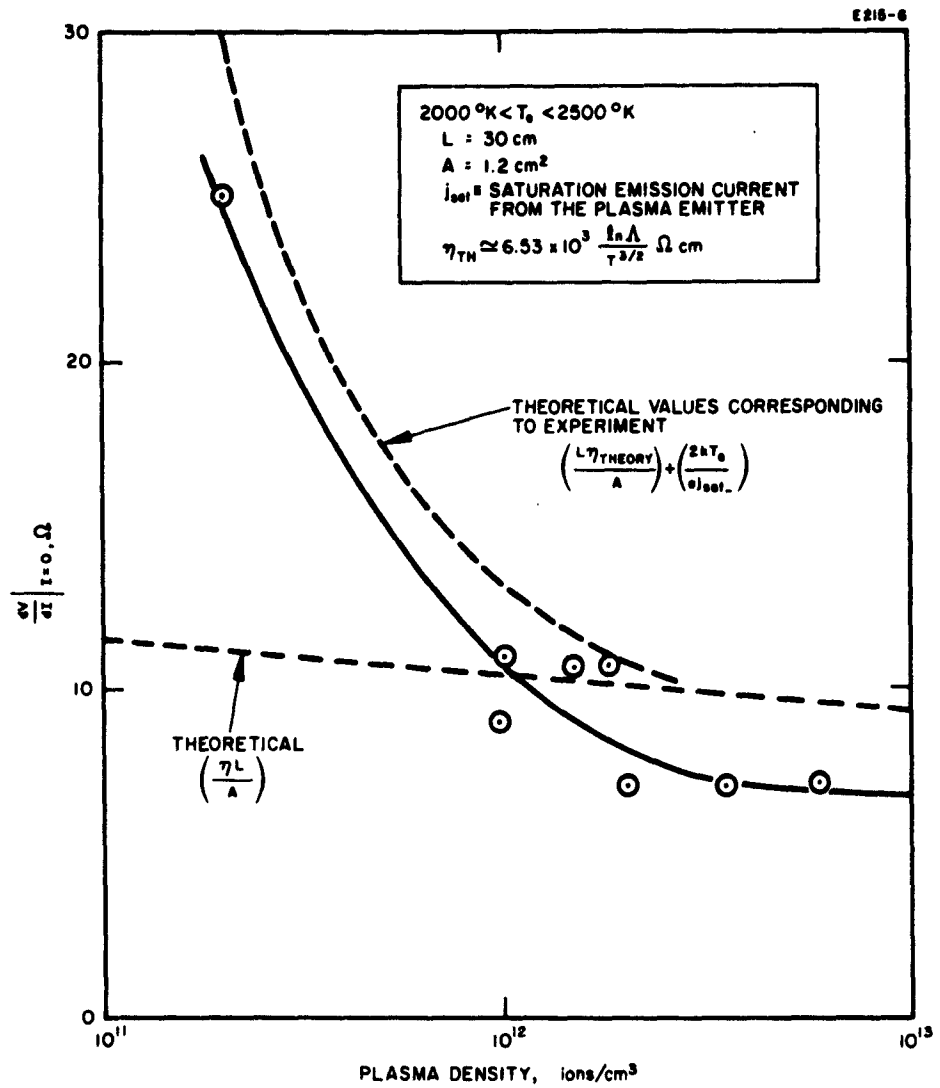


Fig. 29. Slope of I-V characteristics for $I \rightarrow 0$ in cesium plasma tube with two plasma emitters.

C. Measured Plasma Resistivity in the Absence of Ohmic Heating

The resistivity of a highly ionized quiescent cesium plasma was measured by measuring the I-V characteristic of the two plasma emitter system, for plasma densities extending from 5×10^{11} to 6×10^{12} ions/cm³, and an electron temperature between 2200 and 2500°K. As indicated in the preceding section, the reliable evaluation of the volume resistivity should be limited to those experimental conditions in which the contribution of the sheath effect is much smaller than the volume resistivity. In this report, therefore, only those measurements requiring correction due to sheath effects smaller than 25 to 30% are given in Table II, together with the corresponding plasma density and the emitter temperature.

Since the degree of ionization was greater than 30% for these measurements and since these measurements were made for zero conduction current, the contribution of electron-neutral atoms or of plasma heating should be absent. The resistivity of the plasma under these conditions should result predominantly from long range electron-electron and electron-ion Coulomb interactions. Thus the theoretical expression for the resistivity of a fully ionized plasma as shown in (3) should be applicable. In these measurements, the axial plasma density distribution was measured with the available three sets of Langmuir probes. Densities at the midplane of the two emitter systems were compared with the density measured positions 10 cm on both sides of the midplane. These measurements showed that the plasma density distribution between these probes was essentially uniform within 20% up to the density on the order of 5×10^{12} ions/cm³. Since the density dependence appears only in the $\ln \Lambda$ in such a manner that the resistivity is proportional to $\ln(1/n_e)^{1/2}$, the maximum density variation of 20% among three sets of probes has very little effect on the determination of the volume resistivity.

A comparison between the measured and theoretical plasma resistivities is shown in Table II and plotted as a function of the density in Fig. 30. This comparison shows that the experimental values (six out of eight points) are generally 20 to 40% smaller (except for two points which showed agreement within 15%). Considering that the derivation of Spitzer's equation is not exact, this agreement between theory and experiment can be considered satisfactory.

In summary, we can state that our experimental results have shown that the resistivity of a highly ionized quiescent plasma is adequately predicted by Spitzer's formula and that the Coulomb collision cross section used in Spitzer's calculations is reliable.

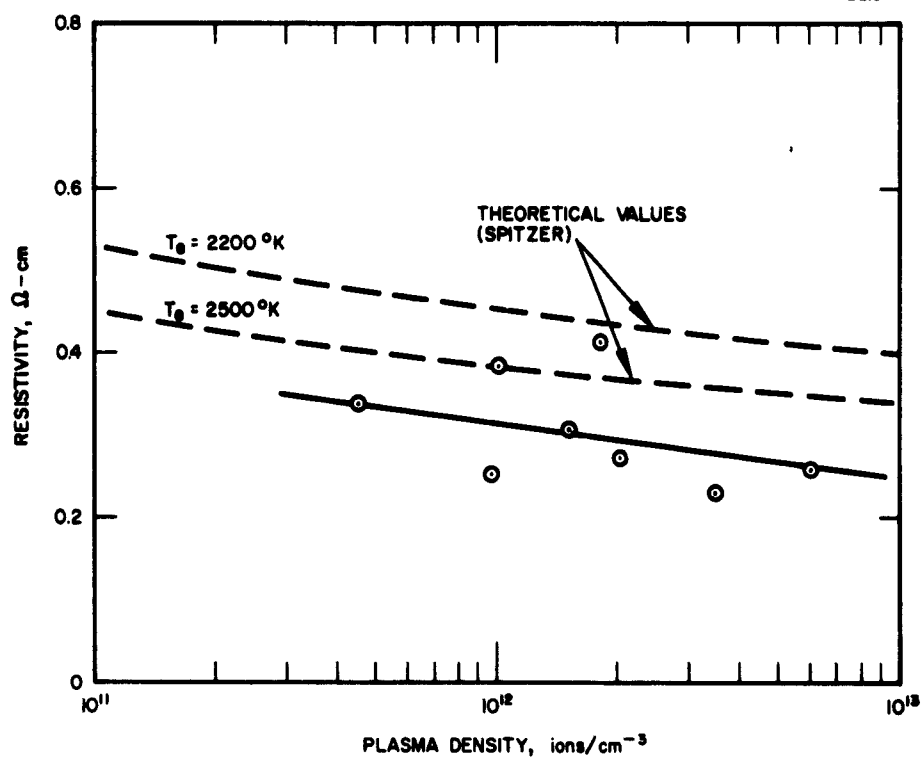


Fig. 30. Measurement of resistivity of highly ionized plasma versus plasma density.

TABLE II

Comparison of Measured and Theoretical
Plasma Resistivities

n_+ $\frac{\text{ions}}{\text{cm}^3}$	T_e , $^{\circ}\text{K}$	η_{exp} , $\Omega\text{-cm}$	η_{theory} , $\Omega\text{-cm}$	$\frac{\eta_{\text{exp}}}{\eta_{\text{theory}}}$
5×10^{11}	2300	0.34	0.45	0.75
9.6×10^{11}	2250	0.25	0.43	0.58
1×10^{12}	2200	0.39	0.45	0.87
1.5×10^{12}	2240	0.31	0.43	0.72
1.8×10^{12}	2300	0.41	0.42	0.98
2.0×10^{12}	2400	0.25	0.39	0.64
3.5×10^{12}	2350	0.23	0.38	0.61
6.0×10^{12}	2420	0.260	0.37	0.70

VII. FORMATION OF CESIUM PLASMA AND MEASUREMENT OF THE PROBABILITY OF NEUTRALIZATION K_n OF Cs^+ ON A TANTALUM SURFACE IN A ONE-EMITTER SYSTEM

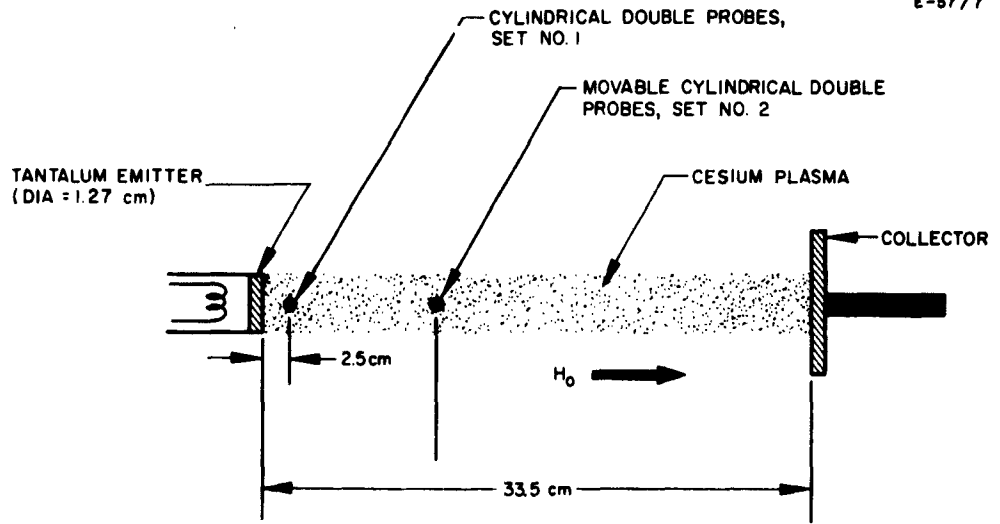
A. Statement of the Problem

The dynamics of cesium plasma generation and loss in a two-emitter system has been analyzed and was reported previously.⁴ Measurements performed with two-emitter systems at relatively low plasma densities ($n_+ < 10^{12}$ ions/cm³), where ion losses due to the volume recombination are negligible, indicate that the probability of neutralization K_n of Cs^+ on hot tantalum is substantially lower than that predicted by the Saha-Langmuir equation. Analysis of the cesium plasma formation has recently been extended to the one-plasma-emitter systems (Fig. 31). The theory shows that the steady-state plasma formation in a one-emitter system is strongly dependent on K_n ; a simple experimental evaluation of K_n is possible when the temperature of the emitter is lowered so that a positive space charge sheath is formed near the emitter surface. This section will describe the theory of cesium plasma formation and summarize the results of the measurements of K_n for Cs^+ on a tantalum surface in a one-emitter system.

B. Method of Measurement

The one-emitter system (see Fig. 31) used for the evaluation of K_n was developed during Phase I of this contract for the study of the low-frequency oscillations observed in a cesium plasma column.⁴ This apparatus consists of a plasma emitter and a collector electrode immersed in a homogeneous axial uniform magnetic field (indicated by H_0 in Fig. 31) and placed in a vacuum tight enclosure. The cesium vapor pressure in this enclosure is controlled by admitting an excess of cesium metal into the apparatus after thorough outgassing and by accurately controlling the temperature of the walls. Direct measurement of the cesium vapor pressure is made during operation by measuring the saturation of the Cs^+ ion emission from a hot tungsten filament installed in the enclosure.

In the apparatus of Fig. 31, ions are emitted by contact ionization of the cesium on the hot tantalum disk; thermionic emission of electrons takes place simultaneously from the same disk. If the electron emission rate is sufficient to neutralize the ions, a plasma will be generated continuously at one end of the plasma column at a rate controlled by the neutral cesium vapor pressure. The plasma is confined magnetically into a well defined column 30 cm long between the emitter and collector. Two sets of double probes located in the plasma column (shown in Fig. 31) measure the ion or plasma density.



H_0 = HOMOGENOUS, AXIAL, DC MAGNETIC FIELD

Fig. 31. One-emitter cesium plasma generator for the measurement of K_n of Cs^+ on tantalum surface.

For the measurement of K_n , the collector is generally biased a few volts negatively with respect to the plasma so that only ions are attracted to the collector. Therefore, the ions generated at the plasma emitter in a low density plasma (negligible volume recombination) diffuse to the collector, and the major portion of the ions are lost there if the rate of electron emission is sufficient to prevent formation of a positive space charge sheath near the emitter surface. On the other hand, if the electron emission rate is inadequate to prevent ion sheath formation (because the plasma emitter is insufficiently heated), the plasma potential becomes positive with respect to the emitter. Since the Cs^+ ions are initially emitted from the tantalum surface with a half Maxwellian velocity distribution, some of the slow Cs^+ ions are reflected back to the plasma emitter in the presence of a positive plasma potential. When they come in contact with the hot tantalum surface, some of these reflected ions are re-emitted as ions; other are neutralized on the surface and escape from the emitter as neutral atoms. The fraction of reflected Cs^+ ions which are neutralized is equal to the probability of neutralization K_n . As the plasma emitter temperature is lowered, the plasma potential becomes more positive with respect to the emitter; the rate of Cs^+ ion loss because of neutralization on the emitter surface increases because greater portions of Cs^+ ions are reflected back to the emitter. Simultaneously, as the plasma becomes more positive with respect to the emitter, the number of Cs^+ ions injected from the emitter into the plasma decreases because of the positive potential wall encountered by the ions in the emitter sheath. Thus the plasma density also decreases.

The following section will show that K_n can be related to the plasma density, the emitter temperature, and the cesium neutral density. The expression which can be used for the experimental determination of K_n is thus derived from the ion and electron conservation conditions. Experimental evaluation of K_n over a limited range of emitter temperatures is then made. The following section will show that the values of K_n measured with the one-emitter system are consistent with those obtained with the two-emitter cesium plasma systems and are lower than those predicted theoretically by the Saha-Langmuir equation.

C. Formation of Cesium Plasma in a One-Emitter System with a Floating Collector

The analysis of cesium plasma formation in a one-emitter system is performed on an idealized infinite parallel plane model under the following assumptions: (1) plasma density is uniform; (2) ions and electrons are emitted only from the plasma emitter; (3) all ions which come in contact with the collector surface are completely neutralized; (4) volume recombination is negligible. A strong dc magnetic field was used to restrict the electron movement along the magnetic field line; the thickness of space charge sheaths at the emitter and the collector is usually very small compared with

either the plasma column diameter or length. For these reasons, the simplified infinite parallel plane model should represent the actual cylindrical plasma. Other assumptions given above are generally consistent with the conditions encountered in the experiment.

The axial potential distribution in the one-emitter system for the conditions appropriate for the evaluation of K_n is shown in Fig. 32. Since the basic procedure for the present analysis is very closely related to the theory of a cesium plasma in two-emitter systems which was treated in detail in an earlier report,¹⁷ only an outline of the derivation will be presented here. The basic equations are the equations of conservation of electrons and ions.

1. Conservation of Ions

Applying the condition of conservation of ions and following the same analytical procedure as for the theory of a two-emitter system,¹⁷ we obtain the following expression:

$$K_i n_o \left(\frac{\bar{v}_o}{4} \right) = n_+ \left(\frac{\bar{v}_+}{4} \right) \left\{ \left[1 - 2 \left(e^{\frac{eV_p}{kT_+}} - 1 \right) \right] K_n + 1 \right\} \quad (31)$$

where

$$\left(\frac{\bar{v}_+}{\bar{v}_o} \right) = \sqrt{\frac{T_+}{T_o}}$$

n_+ \equiv ion density in the plasma column

n_o \equiv cesium neutral density

K_i \equiv probability of ionization of neutral cesium atom incident on the plasma emitting surface

K_n \equiv probability of neutralization of a cesium ion incident on the plasma emitting surface

V_p \equiv plasma potential (zero potential is chosen as the surface potential of the plasma emitter.)

T_+ \equiv ion temperature

T_o \equiv temperature of neutral cesium atoms

e \equiv absolute electron charge

k \equiv Boltzmann constant

\bar{v}_o \equiv mean thermal velocity of neutral cesium atoms

\bar{v}_+ \equiv mean thermal velocity of Cs^+ ions.

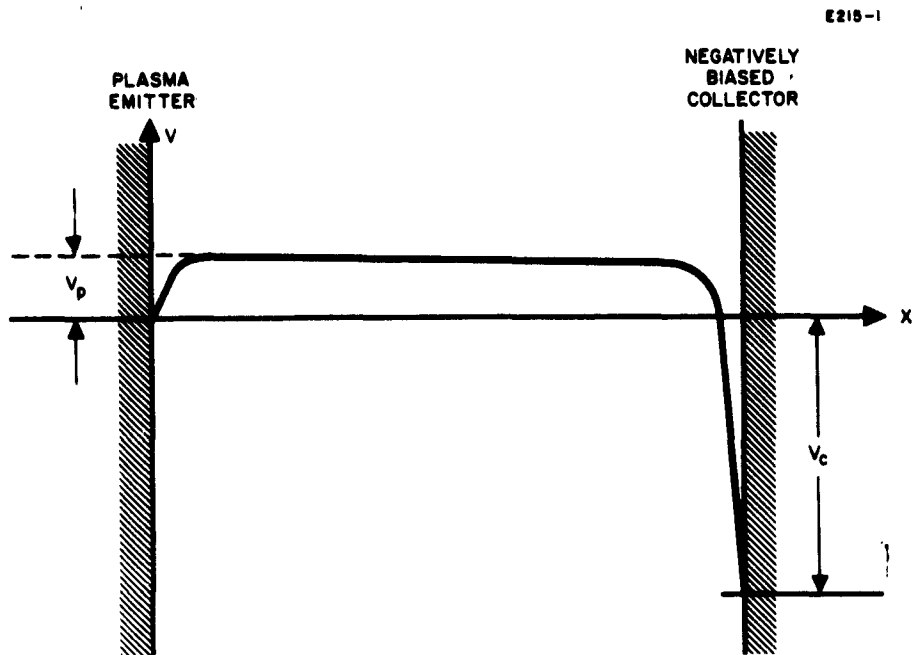


Fig. 32. Axial potential distribution of the plasma column in a single emitter system.

In writing this equation it is assumed that the plasma electron temperature and density are uniform over the entire plasma region. The LHS of (31) represents the ion generation rate, whereas the RHS represents the rate of ion losses.

2. Conservation of Electrons

From a consideration of the electron conservation condition for a floating collector such as that used for these experiments, a simple expression can be derived

$$j_{\text{sat}_-} = en_- \left(\frac{\bar{v}_+}{4} + \frac{\bar{v}_-}{4} e^{-\frac{eV}{kT}} \right) \quad (32)$$

where

- j_{sat_-} \equiv saturation current density available from n_-
- n_- \equiv electron density
- \bar{v}_- \equiv mean thermal electron velocity
- T_- \equiv electron temperature.

In the plasma region, because of the quasi-neutrality condition, $n_- = n_+$. It can be shown from the condition of conservation of energy that $T_- = T_+$. $T_+ = T_e$ where T_e is the plasma emitter temperature.

A considerable simplification can be achieved by defining the following normalized parameters:

$$\left. \begin{aligned} \phi &= \frac{n_+}{N_+} \\ \theta &= \frac{j_{\text{sat}_-}}{eN_+ \left(\frac{\bar{v}_+}{4} \right)} \\ \epsilon &= \left(\frac{m_-}{M_+} \right)^{1/2} = 1/500 \end{aligned} \right\} \quad (32)$$

where

$$N_+ = K_i n_o \sqrt{\frac{T_o}{T_+}}$$

$$m_- \equiv \text{mass of an electron}$$

$$M_+ \equiv \text{mass of a cesium ion.}$$

It should be noted that the plasma density for $V_p = 0$ is related to N_+ in the following manner:

$$n_+ (V_p = 0) = \frac{N_+}{(1 + K_n)} \quad (33)$$

Thus for $K_n \ll 1$, $n_+ (V_p = 0) \approx N_+$ which is the maximum plasma density which can be obtained for a given cesium neutral density.

Equations (31) and (32) are combined to eliminate the plasma potential V_p ; introducing normalized parameters defined above, the equation from which the formation of the plasma as well as K_n in a one-emitter system are estimated reduces to a simple quadratic form:

$$\phi^2 + \phi \left[\frac{\theta - \theta K_n + \epsilon}{2K_n - \epsilon} \right] - \left[\frac{\theta}{2K_n - \epsilon} \right] = 0. \quad (34)$$

By solving for ϕ , the plasma density as a function of θ (or j_{sat}) or the plasma emitter temperature can be estimated for a given value of K_n . Conversely, for a measured ϕ and θ , K_n can be estimated. The numerical calculation has been performed using (34); comparisons with experimental data have been made and will be described below.

3. Comparison between Theory and Experiments on the Formation of Plasma in a One-Emitter System

Before evaluating K_n directly, we shall compare the effect of the plasma emitter temperature on the plasma density for a number of fixed cesium neutral pressures. By simple rearrangement of (34), ϕ can be directly evaluated as a function of K_n and θ .

$$\phi = \sqrt{\left(\frac{\beta}{2}\right)^2 + a} - \left(\frac{\beta}{2}\right) \quad (35)$$

where

$$\beta = \frac{\theta(1 - K_n) + \epsilon}{(2K_n - \epsilon)} \quad (36)$$

$$\alpha = \frac{\theta}{(2K_n - \epsilon)}$$

Theoretical values of ϕ based on these equations have been calculated as a function of θ for the three values of K_n (0.01, 0.03, and 0.10). These numerical results have shown clearly that steady-state plasma formation in a one-emitter system at lower emitter temperatures strongly depends on the value of K_n . As was described earlier, the rate of ion loss to the plasma emitter is a function of K_n ; thus, the general behavior of ϕ as a function of θ can easily be understood. For smaller values of K_n , the plasma potential may become more positive than for larger K_n and still maintain a desired level of plasma density. Conversely, the smaller K_n , the smaller the j_{sat} or T_e required to obtain a given plasma density for a fixed cesium vapor pressure.

For purposes of comparison, the measured data for $N_+ = 6 \times 10^{10}$ ions/cm³ and 1.5×10^{10} ions/cm³ are normalized in the manner defined by (32) and are shown in Fig. 33. In this figure the normalized plasma density $\phi = n_+/N_+$ is plotted as a function of the normalized emitter saturation current $\theta = j_{sat}/eN_+(v_-/4)$ (or the emitter temperature). As can be seen, the effect of the emitter temperature on the formation of the plasma in a one-emitter cesium plasma generator behaves generally as predicted by the theory. The experimental points corresponding to higher plasma density ($N_+ = 6.0 \times 10^{10}$ ions/cm³) show excellent agreement with theory. Other results corresponding to $N_+ = 1.5 \times 10^{10}$ ions/cm³ show considerable discrepancy for a small ϕ where ϕ drops very sharply as the decreasing function of θ . For $N = 1.5 \times 10^{10}$, $\phi < 0.2$ corresponds to $n_+ < 3 \times 10^9$ ions/cm³ where the measurement of plasma densities by a probe becomes unreliable. Except for this one point corresponding to $n_+ < 2 \times 10^9$ ions/cm³, it is observed in Fig. 33 that experimental points are generally located in the area where $K_n < 0.03$. This result suggests, therefore, the possibility of evaluating K_n from various experimental points shown in Fig. 33 using (34) as a function of the measured parameters ϕ and θ .

D. Experimental Evaluation of the Probability of Neutralization K_n of Cesium on Hot Tantalum

In the preceding sections we have shown that the plasma formation in one emitter is strongly influenced by K_n and that a simple experimental evaluation is possible when the temperature of the emitter is lowered so that a positive space charge sheath is formed near the emitter surface.

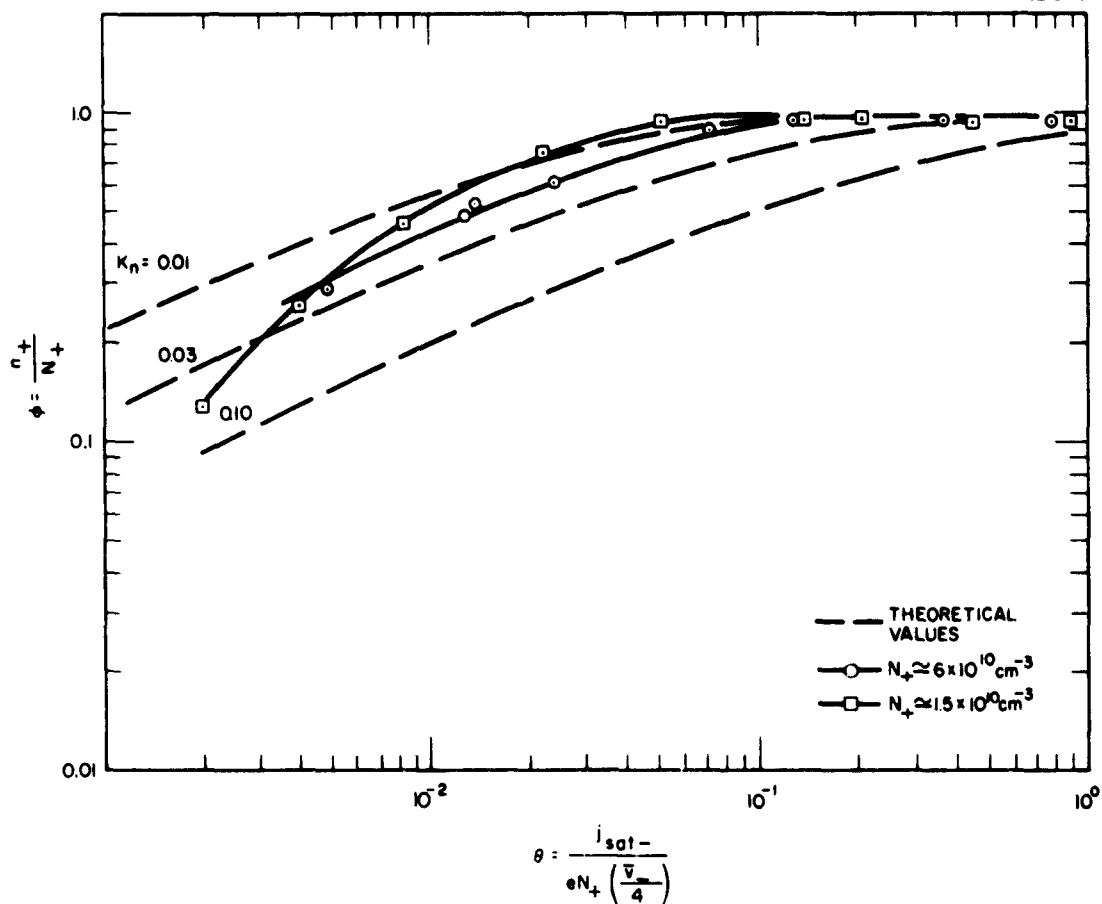


Fig. 33. Comparison of the theoretical and experimental normalized plasma density as a function of the normalizer emitter temperature for $n_+ \approx 6 \times 10^{10}$ and 1.5×10^{10} ions/cm³.

It can be seen from the data shown in Fig. 33 that ϕ (or n_+) approaches unity as θ (or j_{sat_-}) is increased. This effect, as mentioned earlier, results primarily from the lowering of the plasma potential and consequently from the decrease in the rate of Cs^+ ion neutralization on the emitter surface. For the direct evaluation of K_n , we must select a region in which the effect of the surface neutralization becomes an important factor. For this purpose we shall arbitrarily select $\phi < 0.8$ as the upper limit for which K_n is to be evaluated directly. Calculation of K_n can also be made from a rigorous evaluation of K_n through (34). The estimated value of K_n for the one-emitter system as a function of the emitter temperature has been plotted in Fig. 34, together with those values obtained previously from a two-emitter system (also for Cs^+ on a tantalum emitter) and from the Saha-Langmuir equation.

The values obtained from the Saha-Langmuir equation based on a quasi-thermodynamic equilibrium were derived in the previous report on tantalum emitters¹⁷; these values, in which $K_n > 0.20$, are plotted on Fig. 33 over the temperature range extending from 1800°K to 2000°K. These theoretical values are almost an order of magnitude greater than either $K_n < 0.03$, obtained at $T \cong 2000^\circ\text{K}$ and $n_+ \cong 10^{12}$ ions/cm³ for a two emitter system, or $0.01 < K_n < 0.03$, obtained at $T = 1800^\circ\text{K}$ to 1900°K for a one-emitter system. These latter data therefore consistently lead to the same conclusion as the earlier measurements: that the probability of surface recombination seems much lower than that predicted by the Saha-Langmuir equation.

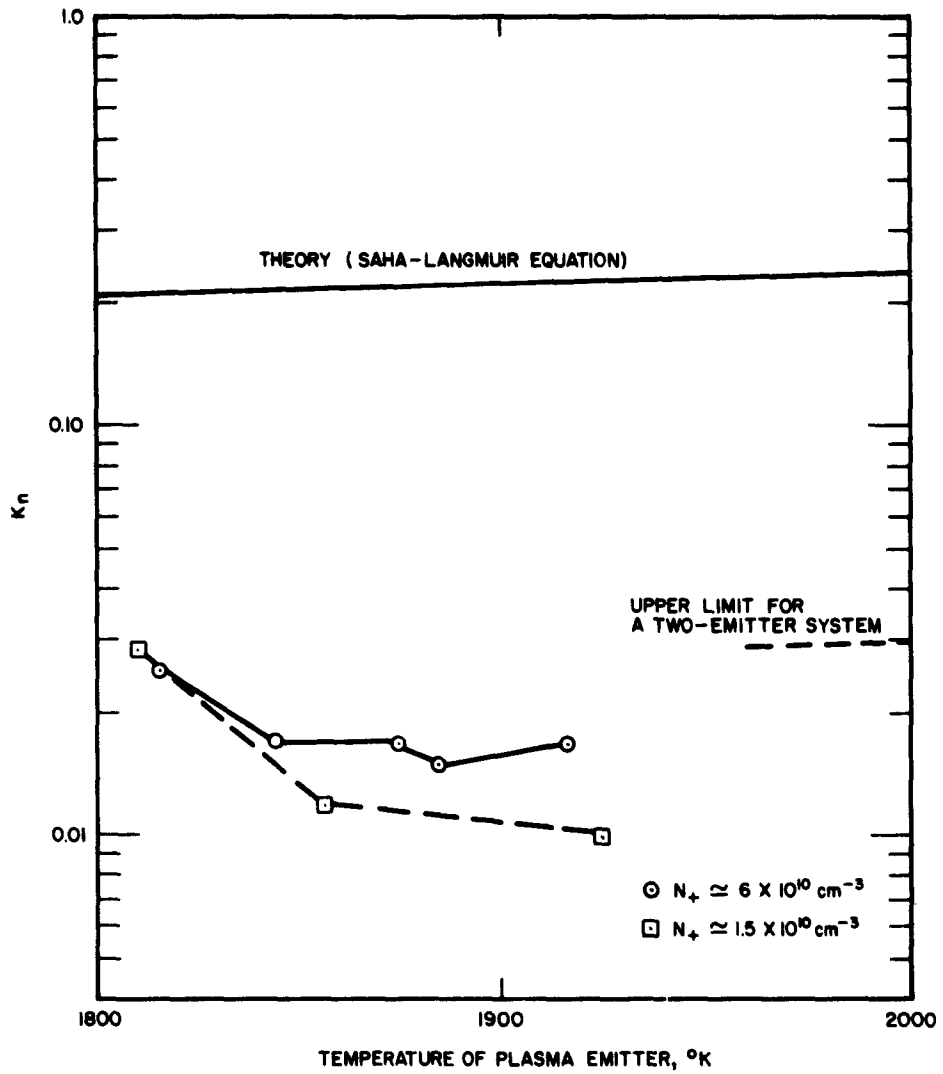


Fig. 34. Probability of neutralization of Cs^+ on hot tantalum surface as a function of the emitter temperature.

REFERENCES

1. K. Hernqvist, Proc. IEEE 51, 748 (1963).
2. L. Malter, E. O. Johnson, and W. M. Webster, RCA Rev. 12, 415 (1951).
3. P. Mazur, J. Appl. Phys. 34, 1611 (1963).
4. R. C. Knechtli and J. Y. Wada, "Cesium Plasma Studies for Thermionic Energy Conversion," Final Report, Phase I, Contract Nonr 3501(00), June 1962.
5. J. Y. Wada and R. C. Knechtli, Proc. IRE 49, 1926 (1961).
6. J. Y. Wada and R. C. Knechtli, "Cesium Plasma Studies for Thermionic Energy Conversion," Semi-Annual Technical Summary Report, Phase II, Contract Nonr 3501(00), December 1962.
7. G. D. Boyd, R. W. Gould, and L. M. Field, Phys. Rev. 109, 1393 (1958).
8. O. Buneman, Phys. Rev. 115, 503 (1959).
9. B. D. Fried and R. W. Gould, Phys. Fluids 4, 139 (1961).
10. W. D. Getty, Technical Report No. 407, Research Laboratory of Electronics, MIT, January 9, 1963.
11. D. Bohm and E. P. Gross, Phys. Rev. 75, 1851 (1949); A. V. Haeff, Proc. IRE 37, 4 (1949); J. R. Pierce, J. Appl. Phys. 19, 231 (1948).
12. J. M. Dawson, Phys. Rev. 113, 303 (1959); J. M. Dawson, Phys. Fluids 5, 445 (1962).
13. R. W. Gould and A. W. Trivelpiece, Proc. Inst. Elect. Engrs. 105B, 516 (1958); J. Appl. Phys. 30, 1787 (1959).
14. I. B. Bernstein and S. K. Trehan, Nuclear Fusion 1, 3 (1960).
15. N. D'Angelo and R. W. Motley, Technical Memorandum No. 153, Plasma Physics Laboratory, Princeton University, June 1962.
16. L. Spitzer, Physics of Fully Ionized Gases (Interscience, New York, 1956), Eq. (5-37).
17. R. C. Knechtli and J. Y. Wada, "Cesium Plasma Studies for Thermionic Energy Conversion," Second Semi-Annual Technical Summary Report, Contract Nonr 3501(00), April 1962.

NONR 3501(00)
Office of Naval Research
CESIUM PLASMA STUDIES FOR THERMIONIC ENERGY CONVERSION
Final Report - June 1963, 91 pp. 34 illus.

Wada, J. Y., and
Knechtli, R. C.
NONR 3501(00)
Office of Naval Research
CESIUM PLASMA STUDIES FOR THERMIONIC ENERGY CONVERSION
Final Report - June 1963, 91 pp. 34 illus.

The processes of thermalization of fast electrons injected into a highly ionized plasma through a plasma sheath have been investigated. Our measurements of the plasma electron temperature have shown that the energy transfer from the fast electrons injected into a plasma to the slow electrons of this plasma takes place at a faster rate than can be accounted for by collision. An effective thermalization of the injected electrons is obtained even when collisions are negligible. The mechanism of the energy transfer and thermalization in the absence of collision (determined from the noise spectra measurements) appears to be a collective interaction between the fast injected electrons and a multiplicity mode of electrostatic plasma waves. This observed fast rate of thermalization seems to be of the same nature as those believed to occur in low voltage arc cesium plasma thermionic energy converters. The results of our investigation thus lead to an appropriate explanation for the process of thermalization of fast electrons found in these cesium plasma converters.

The processes of thermalization of fast electrons injected into a highly ionized plasma through a plasma sheath have been investigated. Our measurements of the plasma electron temperature have shown that the energy transfer from the fast electrons injected into a plasma to the slow electrons of this plasma takes place at a faster rate than can be accounted for by collision. An effective thermalization of the injected electrons is obtained even when collisions are negligible. The mechanism of the energy transfer and thermalization in the absence of collision (determined from the noise spectra measurements) appears to be a collective interaction between the fast injected electrons and a multiplicity mode of electrostatic plasma waves. This observed fast rate of thermalization seems to be of the same nature as those believed to occur in low voltage arc cesium plasma thermionic energy converters. The results of our investigation thus lead to an appropriate explanation for the process of thermalization of fast electrons found in these cesium plasma converters.

The resistivity of highly ionized cesium plasma has been measured for plasma densities ranging from 5×10^{11} to 6×10^{12} ions/cm³ and for electron temperatures between 2000 and 2500°K. The measured values of resistivity were found to be in good agreement with those theoretically predicted by Spitzer. The Coulomb collision cross section for cumulative small angle deflections as calculated by Spitzer is therefore a good estimate of the actual cross section, since it has been found to lead to a valid theoretical expression for the plasma resistivity. Thus, these results justify the use of Spitzer's results for estimating the internal voltage drop and the ohmic plasma heating due to Coulomb collisions as they occur in thermionic energy converters.

The resistivity of highly ionized cesium plasma has been measured for plasma densities ranging from 5×10^{11} to 6×10^{12} ions/cm³ and for electron temperatures between 2000 and 2500°K. The measured values of resistivity were found to be in good agreement with those theoretically predicted by Spitzer. The Coulomb collision cross section for cumulative small angle deflections as calculated by Spitzer is therefore a good estimate of the actual cross section, since it has been found to lead to a valid theoretical expression for the plasma resistivity. Thus, these results justify the use of Spitzer's results for estimating the internal voltage drop and the ohmic plasma heating due to Coulomb collisions as they occur in thermionic energy converters.

Measurements of the probability of the neutralization of cesium ions on a hot refractory metal emitter (one of the important parameters which affects the rate of ion loss, the economy of the discharge, and the potential distribution in cesium plasma thermionic energy converters) have been made using a single emitter cesium plasma tube. The results have agreed consistently with earlier experiments (conducted with a two emitter tube), indicating that the probability of the neutralization of cesium ions on refractory metal surfaces and on tantalum in particular is substantially lower than predicted by the Saha-Langmuir equation.

Measurements of the probability of the neutralization of cesium ions on a hot refractory metal emitter (one of the important parameters which affects the rate of ion loss, the economy of the discharge, and the potential distribution in cesium plasma thermionic energy converters) have been made using a single emitter cesium plasma tube. The results have agreed consistently with earlier experiments (conducted with a two emitter tube), indicating that the probability of the neutralization of cesium ions on refractory metal surfaces and on tantalum in particular is substantially lower than predicted by the Saha-Langmuir equation.

Wada, J. Y., and
Knechtli, R. C.
NONR 3501(00)
Office of Naval Research
CESIUM PLASMA STUDIES FOR THERMIONIC ENERGY CONVERSION
Final Report - June 1963, 91 pp. 34 illus.

Wada, J. Y., and
Knechtli, R. C.
NONR 3501(00)
Office of Naval Research
CESIUM PLASMA STUDIES FOR THERMIONIC ENERGY CONVERSION
Final Report - June 1963, 91 pp. 34 illus.

The processes of thermalization of fast electrons injected into a highly ionized plasma through a plasma sheath have been investigated. Our measurements of the plasma electron temperature have shown that the energy transfer from the fast electrons injected into a plasma to the slow electrons of this plasma takes place at a faster rate than can be accounted for by collision. An effective thermalization of the injected electrons is obtained even when collisions are negligible. The mechanism of the energy transfer and thermalization in the absence of collision (determined from the noise spectra measurements) appears to be a collective interaction between the fast injected electrons and a multiplicity mode of electrostatic plasma waves. This observed fast rate of thermalization seems to be of the same nature as those believed to occur in low voltage arc cesium plasma thermionic energy converters. The results of our investigation thus lead to an appropriate explanation for the process of thermalization of fast electrons found in these cesium plasma converters.

The processes of thermalization of fast electrons injected into a highly ionized plasma through a plasma sheath have been investigated. Our measurements of the plasma electron temperature have shown that the energy transfer from the fast electrons injected into a plasma to the slow electrons of this plasma takes place at a faster rate than can be accounted for by collision. An effective thermalization of the injected electrons is obtained even when collisions are negligible. The mechanism of the energy transfer and thermalization in the absence of collision (determined from the noise spectra measurements) appears to be a collective interaction between the fast injected electrons and a multiplicity mode of electrostatic plasma waves. This observed fast rate of thermalization seems to be of the same nature as those believed to occur in low voltage arc cesium plasma thermionic energy converters. The results of our investigation thus lead to an appropriate explanation for the process of thermalization of fast electrons found in these cesium plasma converters.

The resistivity of highly ionized cesium plasma has been measured for plasma densities ranging from 5×10^{11} to 6×10^{12} ions/cm³ and for electron temperatures between 2000 and 2500°K. The measured values of resistivity were found to be in good agreement with those theoretically predicted by Spitzer. The Coulomb collision cross section for cumulative small angle deflections as calculated by Spitzer is therefore a good estimate of the actual cross section, since it has been found to lead to a valid theoretical expression for the plasma resistivity. Thus, these results justify the use of Spitzer's results for estimating the internal voltage drop and the ohmic plasma heating due to Coulomb collisions as they occur in thermionic energy converters.

The resistivity of highly ionized cesium plasma has been measured for plasma densities ranging from 5×10^{11} to 6×10^{12} ions/cm³ and for electron temperatures between 2000 and 2500°K. The measured values of resistivity were found to be in good agreement with those theoretically predicted by Spitzer. The Coulomb collision cross section for cumulative small angle deflections as calculated by Spitzer is therefore a good estimate of the actual cross section, since it has been found to lead to a valid theoretical expression for the plasma resistivity. Thus, these results justify the use of Spitzer's results for estimating the internal voltage drop and the ohmic plasma heating due to Coulomb collisions as they occur in thermionic energy converters.

Measurements of the probability of the neutralization of cesium ions on a hot refractory metal emitter (one of the important parameters which affects the rate of ion loss, the economy of the discharge, and the potential distribution in cesium plasma thermionic energy converters) have been made using a single emitter cesium plasma tube. The results have agreed consistently with earlier experiments (conducted with a two emitter tube), indicating that the probability of the neutralization of cesium ions on refractory metal surfaces and on tantalum in particular is substantially lower than predicted by the Saha-Langmuir equation.

Measurements of the probability of the neutralization of cesium ions on a hot refractory metal emitter (one of the important parameters which affects the rate of ion loss, the economy of the discharge, and the potential distribution in cesium plasma thermionic energy converters) have been made using a single emitter cesium plasma tube. The results have agreed consistently with earlier experiments (conducted with a two emitter tube), indicating that the probability of the neutralization of cesium ions on refractory metal surfaces and on tantalum in particular is substantially lower than predicted by the Saha-Langmuir equation.

DISTRIBUTION LIST

	<u>No. of Copies</u>
Office of Naval Research Power Branch (Code 429) Department of the Navy Washington 25, D. C.	4
Commanding Officer Office of Naval Research Branch Office 1030 E. Green Street Pasadena, California	1
U.S. Naval Research Laboratory Technical Information Division Washington 25, D. C.	6
Commanding Officer Office of Naval Research Branch Office Box 39 Navy No. 100 Fleet Post Office New York, New York	2
Office of Technical Services Department of Commerce Washington 25, D. C.	1
Armed Services Technical Information Agency Arlington Hall Station Arlington 12, Virginia	10
National Aeronautics and Space Administration 1520 H Street, NW Washington 25, D. C. Attn: James J. Lynch	1
National Aeronautics and Space Administration Lewis Research Center 2100 Brookpark Road Cleveland 35, Ohio Attn: H. Schwartz	1
Roland Breitwieser	1
Bernard Lubarsky	1
W. LaGrey	1
R. P. Migra	1

Chief of Naval Operations (OP-07G) Department of the Navy Washington 25, D. C.	1
Commandant, U. S. Marine Corps Code CSY-3 Headquarters, Marine Corps Washington 25, D. C.	1
Chief, Bureau of Ships Department of the Navy Washington 25, D. C. Attn: Code 342B	2
Code 1500, LCDR J.H. Weber	1
Code 456B, Mr. V. Gardner	1
Code 210L	2
U. S. Atomic Energy Commission Division of Reactor Development Washington 25, D. C. Attn: SNAP Reactor Branch	1
Direct Conversion Branch	1
Army Reaction, Water Systems Branch	1
Isotopic Power Branch	1
Aeronautical Systems Division ASRMFP-2 Wright-Patterson Air Force Base, Ohio	1
Air Force Cambridge Research Center (CRZAP) L. G. Hanscom Field Bedford, Massachusetts	1
Power Information Center University of Pennsylvania Moore School Building 200 South 33rd Street Philadelphia 4, Pennsylvania	1
Director of Special Projects (SP-001) Department of the Navy Washington 25, D. C.	1
Los Alamos Scientific Laboratory P. O. Box 1663 Los Alamos, New Mexico Attn: Dr. George M. Grover	1

Argonne National Laboratory 9700 South Cass Avenue Argonne, Illinois Attn: Aaron J. Ulrich	1
Director, Advanced Research Projects Agency The Pentagon Washington 25, D. C. Attn: Dr. John Huth	4
U. S. Army Signal R. and D. Laboratory Fort Monmouth, New Jersey Attn: Emil Kittl	1
Research Laboratories Library General Motors Corporation General Motors Technical Center P. O. Box 388 Warren, Michigan Attn: Dr. F. Jamerson	1
Atomics International P. O. Box 309 Canoga Park, California Attn: Dr. R. C. Allen	1
General Atomic P. O. Box 608 San Diego 12, California Attn: Dr. R. W. Pidd	1
ARACON Laboratories Virginia Road Concord, Massachusetts Attn: Dr. S. Ruby	1
Ford Instrument Company 3110 Thomas Avenue Long Island City, New York Attn: T. Jarvis	1
Armour Research Foundation 10 W. 35th Street Chicago 16, Illinois Attn: Dr. D. W. Levinson	1

Jet Propulsion Laboratory
California Institute of Technology
4800 Oak Grove Drive
Pasadena, California
Attn: P. Rouklove 1

RCA Laboratories
David Sarnoff Research Center
Princeton, New Jersey
Attn: Dr. P. Rappaport 1

The Martin Corporation
Baltimore 3, Maryland
Attn: Dr. M. Talaat 1

Thermo Electron Engineering Corporation
85 First Avenue
Waltham 54, Massachusetts
Attn: Dr. George Hatsopoulos 1

Hughes Research Laboratories
3011 Malibu Canyon Road
Malibu, California
Attn: Dr. R. C. Knechtli 1

Thompson Ramo Wooldridge, Inc.
7209 Platt Avenue
Cleveland 4, Ohio
Attn: Wm. J. Leovic 1

General Electric Research Laboratory
Schenectady, New York
Attn: Dr. V. C. Wilson 1

The Marquardt Corporation
ASTRO Division
16555 Saticoy Street
Van Nuys, California
Attn: Dr. R. Laubenstein 1

Texas Instruments, Inc.
P. O. Box 5474
Dallas 22, Texas
Attn: Dr. R. A. Chapman 1

University of Denver
Colorado Seminary
Denver Research Institute
Denver 10, Colorado
Attn: Dr. Charles B. Magee 1

Radio Corporation of America
Electron Tube Division
Lancaster, Pennsylvania
Attn: F. G. Block

1

Electro-Optical Systems, Inc.
300 N. Halstead Avenue
Pasadena, California
Attn: Dr. A. O. Jensen

1

General Electric Company
P. O. Box 846
Atomic Product Division
Vallecitos Laboratory
Pleasanton, California
Attn: Robert Scott

1

General Electric Company
Power Tube Division
1 River Road
Schenectady 5, New York
Attn: Mr. D. L. Schaefer

1

Consolidated Controls Corporation
Bethel, Connecticut
Attn: Mr. David Mends

1

Institute for Defense Analysis
1666 Connecticut Avenue, N. W.
Washington, D. C.
Attn: Mr. Robert Hamilton

1

Knolls Atomic Power Laboratories
Schenectady, New York
Attn: Dr. R. Ehrlich

1

Professor J. E. Rowe
Professor and Director
Electron Physics Laboratory
The University of Michigan
3505 East Engineering Building
Ann Arbor, Michigan

1